WYNER-ZIV CODING BASED ON TCQ AND LDPC CODES AND EXTENSIONS TO MULTITERMINAL SOURCE CODING

A Thesis

by

YANG YANG

Submitted to the Office of Graduate Studies of
Texas A&M University
in partial fulfillment of the requirements for the degree of

MASTER OF SCIENCE

August 2004

Major Subject: Electrical Engineering

WYNER-ZIV CODING BASED ON TCQ AND LDPC CODES AND EXTENSIONS TO MULTITERMINAL SOURCE CODING

A Thesis

by

YANG YANG

Submitted to Texas A&M University
in partial fulfillment of the requirements
for the degree of

MASTER OF SCIENCE

Approved as to style and content by:

Zixiang Xiong (Chair of Committee)	
Costas N. Georghiades (Member)	Aniruddha Datta (Member)
Wei Zhao (Member)	Chanan Singh (Head of Department)

August 2004

Major Subject: Electrical Engineering

ABSTRACT

Wyner-Ziv Coding Based on TCQ and LDPC Codes
and Extensions to Multiterminal Source Coding. (August 2004)
Yang Yang, B.S., Tsinghua University
Chair of Advisory Committee: Dr. Zixiang Xiong

Driven by a host of emerging applications (e.g., sensor networks and wireless video), distributed source coding (i.e., Slepian-Wolf coding, Wyner-Ziv coding and various other forms of multiterminal source coding), has recently become a very active research area.

In this thesis, we first design a practical coding scheme for the quadratic Gaussian Wyner-Ziv problem, because in this special case, no rate loss is suffered due to the unavailability of the side information at the encoder. In order to approach the Wyner-Ziv distortion limit $D^*_{WZ}(R)$, the trellis coded quantization (TCQ) technique is employed to quantize the source X, and irregular LDPC code is used to implement Slepian-Wolf coding of the quantized source input $Q(X)$ given the side information Y at the decoder. An optimal non-linear estimator is devised at the joint decoder to compute the conditional mean of the source X given the dequantized version of $Q(X)$ and the side information Y. Assuming ideal Slepian-Wolf coding, our scheme performs only 0.2 dB away from the Wyner-Ziv limit $D^*_{WZ}(R)$ at high rate, which mirrors the performance of entropy-coded TCQ in classic source coding. Practical designs perform 0.83 dB away from $D^*_{WZ}(R)$ at medium rates. With 2-D trellis-coded vector quantization, the performance gap to $D^*_{WZ}(R)$ is only 0.66 dB at 1.0 b/s and 0.47 dB at 3.3 b/s.

We then extend the proposed Wyner-Ziv coding scheme to the quadratic Gaus-

sian multiterminal source coding problem with two encoders. Both direct and indirect settings of multiterminal source coding are considered. An asymmetric code design containing one classical source coding component and one Wyner-Ziv coding component is first introduced and shown to be able to approach the corner points on the theoretically achievable limits in both settings. To approach any point on the theoretically achievable limits, a second approach based on source splitting is then described. One classical source coding component, two Wyner-Ziv coding components, and a linear estimator are employed in this design. Proofs are provided to show the achievability of any point on the theoretical limits in both settings by assuming that both the source coding and the Wyner-Ziv coding components are optimal. The performance of practical schemes is only 0.15 b/s away from the theoretical limits for the asymmetric approach, and up to 0.30 b/s away from the limits for the source splitting approach.

To my parents

ACKNOWLEDGMENTS

I would like to express my deepest gratitude to Dr. Zixiang Xiong for his great patience and enlightening guidance. He is always a source of encouragement throughout my graduate studies. I would like to thank Dr. Wei Zhao for all his kind help without which I could not be where I am today. I would also like to thank Dr. Costas N. Georghiades, and Dr. Aniruddha Datta for serving on my committee. I want to thank my colleagues in the Multimedia Laboratory for sharing their insightful knowledge with me. I am especially grateful to Dr. Vladimir Stanković, Samuel Cheng, and Angelos D. Liveris for their many helpful suggestions and assistance. I also want to express my hearty appreciation to my parents, who gave me not only life, but all their love.

TABLE OF CONTENTS

CHAPTER Page

LIST OF TABLES

LIST OF FIGURES

FIGURE Page

FIGURE Page

CHAPTER I

INTRODUCTION

Distributed source coding, ignited by the landmark paper by Slepian and Wolf [1], targets at various types of applications that deal with the transmission of multiple sources over multiple channels, to a single destination (e.g., distributed sensor networks and wireless video). Compared to conventional point-to-point communication, performance gains are promised with distributed source coding at the cost of increased complexity. From the lossless Slepian-Wolf coding problem, to the lossy Wyner-Ziv coding problem, and to the more general multiterminal source coding problem, a lot of works have been done to find the theoretical performance limits and to build coding schemes that approach these limits. However, most results are still at the theoretical level, which has limited the potential applications of distributed source coding theory in practice. This thesis focuses on the design of practical codes for distributed source coding. Specifically, Wyner-Ziv code design and multiterminal source code design are the two topics considered in this thesis.

A. Wyner-Ziv Code Design

Wyner-Ziv coding [2] refers to lossy source coding with side information (SCSI) at the decoder. It is more general than the Slepian-Wolf coding [1] problem of lossless SCSI. There is usually a rate loss with Wyner-Ziv coding when compared to lossy coding of source X when the side information Y is available at both the encoder and the decoder (see for example the binary Wyner-Ziv problem in [2]). One exception is

---

The journal model is *IEEE Transactions on Automatic Control.*

when X and Y are jointly Gaussian with MSE measure, there is no rate loss[1] with Wyner-Ziv coding. In this thesis, we only consider this quadratic Guassian case, which is of special interest in practice because many image and video sources can be modeled as jointly Gaussian (after mean subtraction).

Because we are introducing distortion to the source with Wyner-Ziv coding, source coding is needed to quantize X. Usually there is still correlation remaining in the quantized version $Q(X)$ and the side information Y, channel coding (e.g., Slepian-Wolf coding) should be employed to exploit this correlation to reduce the rate from $H(Q(X))$ to $H(Q(X)|Y)$. Thus, Wyner-Ziv coding is a source-channel coding problem. There is quantization loss due to source coding and binning loss due to channel coding. In order to reach the Wyner-Ziv limit, one needs to employ both source codes (e.g., TCQ [4]) that can achieve the granular gain and channel codes (e.g., turbo [5] or LDPC codes [6]) that can approach the Slepian-Wolf limit. In addition, the side information Y can be used in jointly decoding and optimally estimating $\hat{X}$ at the decoder to help reduce the average distortion $E[d(X, \hat{X})]$, especially at low rate.

Zamir and Shamai [7] first outlined some constructive mechanisms for quadratic Guassian Wyner-Ziv coding using a pair of nested lattice codes. Servetto [8] proposed explicit nested lattice constructions based on similar sublattices for the high correlation case. Research on trellis-based nested codes as a way of realizing high-dimensional nested lattice codes has just started recently [9, 10, 11, 12].

Source and channel codes of about the same dimension are utilized in nested lattice [8] or TCQ constructions [11]. However, in this setup, the channel code is not strong enough in the sense that the performance gap of the source code to the

[1]Pradhan, Chou, and Ramchandran [3] recently extended the zero-rate-loss condition for Wyner-Ziv coding to $X = Y + Z$, where Z is independently Gaussian but Y (hence X) could follow more general distributions.

rate-distortion function is much smaller than that of the channel code to the capacity. A Slepian-Wolf coded nested quantization (SWC-NQ) paradigm was proposed in [13] to rectify this shortcoming by following nested quantization with a second layer of binning via Slepian-Wolf coding. At high rate, asymptotic performance limits of SWC-NQ similar to those in classic source coding were established in [13], showing that ideal Slepian-Wolf coded 1-D/2-D nested lattice quantization performs 1.53/1.36 dB worse than the Wyner-Ziv distortion-rate function $D^*_{WZ}(R)$ with probability almost one. Performances close to the corresponding theoretical limits were obtained by using 1-D and 2-D nested lattice quantization, together with irregular LDPC codes for Slepian-Wolf coding.

To further explore the remaining 1.36 dB gap from Slepian-Wolf coded 2-D nested lattice quantization to $D^*_{WZ}(R)$, higher dimensional lattice quantization must be employed. Hence TCQ, an efficient technique to implement higher dimensional lattice quantization, is combined with LDPC codes based Slepian-Wolf coding [14] for Wyner-Ziv coding. The intuition that all the binning should be left to the Slepian-Wolf code, allows the best possible binning (a high dimensional channel code). This limits the performance loss of such a Wyner-Ziv code to that from source coding alone [15]. Some interesting results were reported in [16], where assuming ideal Slepian-Wolf coding and high rate the use of classic quantization seemed to be sufficient. Our combined source-channel coding approach could be viewed as a form of nesting with fixed finite source code dimension and larger channel code dimension. This generalized context can include the turbo-trellis Wyner-Ziv codes introduced in [12], where the source code is a TCQ nested with a turbo channel code. However, the scheme in [12] can be simply classified as a nested one. It performs 1.3 dB away from $D^*_{WZ}(R)$ at 1.0 b/s.

We show that at high rate, SWC-TCQ performs 0.2 dB away from $D^*_{WZ}(R)$.

This 0.2 dB gap is the same as that between the performance of entropy-coded TCQ and the distortion-rate function $D_X(R)$ in classical source coding. This and results in [13] establish the connection between performances of high-rate Wyner-Ziv coding and classic source coding. Practical designs with TCQ, irregular LDPC code based Slepian-Wolf coding and optimal estimation at the decoder can perform 0.83 dB away from $D^*_{WZ}(R)$ at medium bit rates (e.g., $\geq$ 2.3 b/s). With 2-D trellis-coded vector quantization (TCVQ), the performance gap to $D^*_{WZ}(R)$ is only 0.66 dB at 1.0 b/s and 0.47 dB at 3.3 b/s. These results show that our designs come much closer to the theoretical performance limit of Wyner-Ziv coding than any other previously presented designs.

B. Multiterminal Source Code Design

Multiterminal source coding deals with separate lossy encoding and joint decoding of multiple correlated sources. There are two classes of multiterminal problems. If each sensor observes *directly* the source, we have *direct multiterminal source coding* [17, 18]. On the other hand, if each sensor cannot observe directly the source which is to be reconstructed at the decoder, but is rather provided only with one of its noisy versions, then we speak of *indirect (remote) multiterminal source coding* (e.g., the CEO problem [19, 20]).

The multiterminal problem consists of determining *achievable rate region*; that is, the rates at which sources (or, noisy observations) can be separately compressed, so that at the central unit they can be recovered jointly within a target distortion. Though intense research efforts have been conducted in solving multiterminal problems, achievable rate regions, in general, are still unknown; only inner and outer

limits have been provided so far [17, 21, 22, 23][2]. The quadratic Gaussian case was considered in [17, 21, 18] and [20, 24, 25] for the direct and indirect multiterminal problem, respectively. In contrast to the direct problem, where even in this simple case the inner and outer limits do not fully coincide, the latest result [25] shows that the Berger-Tung achievable region is tight in the indirect problem.

Though a lot has already been done in providing the theoretical limits for the multiterminal problems, achievements in designing practical codes that can approach these limits are very modest. Based on the tight limit for indirect multiterminal coding in the symmetric quadratic Gaussian case [25], Pradhan and Ramchandran [26] provided a code design with fixed-rate scalar quantizers and trellis codes. Although capable of trading off transmission rates among two encoders, the design in [26] performs far away from the theoretical limits, especially at low rates. Note that for direct multiterminal coding, no code design has been provided yet.

Inspired by the fact that Wyner-Ziv coding [2] is a special case of multiterminal coding, we proposed in chapter IV an asymmetric coding system for both the direct and indirect multiterminal coding problems that essentially relies on Wyner-Ziv coding. Our main idea is to quantize the first observation and apply Wyner-Ziv coding on the other by using the quantized version of the first as side information in an efficient asymmetric coding system. Specifically, we rely on TCQ for quantizing the first observation and employ SWC-TCVQ for Wyner-Ziv coding of the second. While we can trade off the rates among the two encoders under the distortion constraint in our system, only one rate allocation scheme minimizes the sum-rate. We show that this allocation corresponds to one of the two corner points on the theoretical sum-rate limit given in [20, 24]. The other corner point can be achieved by symmetry

[2]All rate points within the inner limit are achievable, while those outside the outer limit are not.

of the two observations. Hence, our system is limited in the sense that it can only approach the two corner points, that is why we call it *asymmetric coding*. In our practical code design, however, we are faced with several problems. First, the correlation model among observations is different from that in the Wyner-Ziv problem. Second, the decoder can only exploit the correlation among the quantized observations, rather than the actual correlation among the observations. Finally, since the reconstructions are not Gaussian, the linear estimator might not be optimal anymore. We propose solutions that overcome these difficulties, and apply them to our SWC-TCQ/TCVQ scheme. We report results that are significantly better than previously published [26] and come very close to the theoretical limits.

Although the above asymmetric coding approach shows much better results than those of [26], it is limited to approaching only the two corner points on the achievable limit. However, very often, it is needed to vary the rates of individual encoders while keeping the total sum rate constant; that is, to approach any point on the limit. One way of achieving this is the *source splitting method*, first introduced in [27] in the context of asynchronous Slepian-Wolf coding [1]. The main idea is to split two sources into three and to transform any rate point on the sum rate limit for the two-source Slepian-Wolf problem to a corner point for the three-source Slepian-Wolf problem. A practical scheme for Slepian-Wolf coding based on source splitting was proposed recently in [28]. The extension of source splitting from Slepian-Wolf coding to *direct multiterminal source coding* with two encoders is suggested by Zamir, Shamai, and Erez [29]. However, no practical code design was provided.

Based on the idea of [29], we provide a practical coding scheme containing a classical source coding component and two Wyner-Ziv coding components. Entropy-coded TCQ [31] with dithered uniform codebook is employed for classical source coding, and the SWC-TCQ/TCVQ scheme [32] is used in each of the two Wyner-Ziv

coding components. Assuming ideal source coding and ideal Wyner-Ziv coding, we prove that this scheme is capable of achieving any rate point on the theoretical limits for both the direct and indirect multiterminal problems in the quadratic Gaussian setting. Practical designs based on entropy-coded TCQ for source coding and SWC-TCQ/TCVQ for Wyner-Ziv coding significantly outperform those of [26] and come very close to the theoretical limits in both multiterminal problems.

C. Summary of Contribution

The thesis work has advanced our knowledge on fundamental performance limits of practical Wyner-Ziv code designs, bridged the gap between network information theory and practical code design, and deepened our understanding of classical information theory and conventional approaches to point-to-point communications as well. From a practical point of view, the proposed multiterminal source code designs will make a plethora of applications promised by the theory a reality and pave ways for the deployment of distributed sensor networks.

Specific contributions of this thesis include

- We provide a practical code design based on TCQ and LDPC code for Wyner-Ziv coding. This design performs much closer to the theoretical performance limit of Wyner-Ziv coding than any other previously presented design.
  - We succeed to combine TCQ as a powerful source code and irregular LDPC codes as near capacity channel codes for Wyner-Ziv coding, which is a joint source-channel coding problem.
  - We statistically analyze the relationship between the input (the source X to be quantized) and the output (the TCQ indices $Q(X)$) of TCQ. Using the joint statistics of the TCQ input-output pair, we design an optimal

estimation algorithm without the assumption of Gaussian or independent quantization noise.

  - We show that with ideal Slepian-Wolf coding, our design performs only 0.2 dB from the Wyner-Ziv limit. This and results in [13] establish the connection between performances of high-rate Wyner-Ziv coding and classic source coding.

- We design an asymmetric coding scheme for both the quadratic Gaussian direct and indirect multiterminal source coding problems. Our method is capable of achieving the two corner points on the inner sum rate limits in both cases. Practical results show a much smaller performance gap than best known results in [26].

- We propose the first practical coding scheme for multiterminal source coding based on source splitting, which can approach any point on the inner sum rate limits for both the quadratic Gaussian direct and indirect multiterminal problems.

CHAPTER II

PRELIMINARIES

A. Notation

Throughout this thesis, random variables are denoted as capital letters, e.g., X, Y, ..., or possibly with a subscript, hat ($\hat{}$), or tilde ($\tilde{}$), e.g., Y_1, $\hat{Y}$, $\tilde{Y}$, ... They take values from the sets $\mathcal{X}$, $\mathcal{Y}$, ... A length-n vector of samples drawn from a random variable is denoted as the corresponding random variable with a superscript n, e.g., X^n, Y^n, Y_1^n, $\hat{Y}^n$, ... Each of the n samples of a random vector (e.g., $\tilde{Y}_1^n$), are denoted as the corresponding random variable with a subscript identifying its index in the vector (e.g., $\tilde{Y}_{1,1}$), i.e.,

$$\tilde{Y}_1^n = \{\tilde{Y}_{1,0}, \tilde{Y}_{1,1}, \ldots, \tilde{Y}_{1,n-1}\}. \tag{2.1}$$

B. Trellis Coded Quantization

Trellis coded quantization (TCQ) is an efficient way to implement high-dimensional lattice quantization, which is capable of achieving the classical distortion-rate bound as dimension n goes to infinity. It borrows the idea of set partitioning from trellis coded modulation and uses specific designed trellises to construct high-dimensional lattices. TCQ is often referred to as the most powerful source coding technique because it can achieve very good MSE performance at modest complexity.

1. Fixed Rate TCQ

Suppose we need to quantize a continuous source X using rate R bit per sample. TCQ first takes a codebook of size $2^{R+\tilde{R}}$, and partition it into $2^{\tilde{R}+1}$ subsets, each having 2^{R-1} codewords. Normally, $\tilde{R}$ is set to one. Hence, we have four subsets, denoted as D_0,

D_1, D_2, and D_3. They are also referred to as *cosets*, and $B_0 = D_0 \cup D_2$, $B_1 = D_1 \cup D_3$ are called *supersets*. A example of the partitioning procedure is illustrated in Fig. 1. From left to right, the consecutive codewords are labelled D_0, D_1, D_2, D_3, D_0, D_1, D_2, D_3, ... The codewords are denoted as q_i^j, $i = 0, 1, 2, 3$, $j = 0, 1, \ldots, 2^{R-1} - 1$, where i is called *coset index*, and j is called *codeword index*.

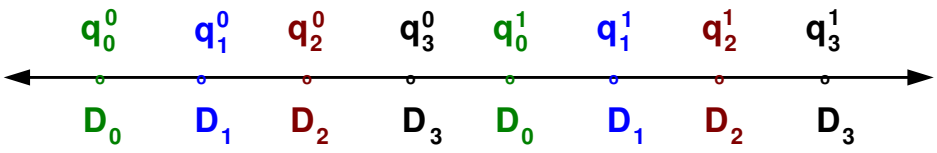

Fig. 1. A example of partitioning of 8 codewords for a 2-bit TCQ.

A *trellis* is in fact a state transition diagram of a finite-state machine. In other words, a trellis is a mapping from the current state $S_{current}$ and input message I to the next state S_{next} and output message O, i.e., $(S_{current}, I) \longrightarrow (S_{next}, O)$.

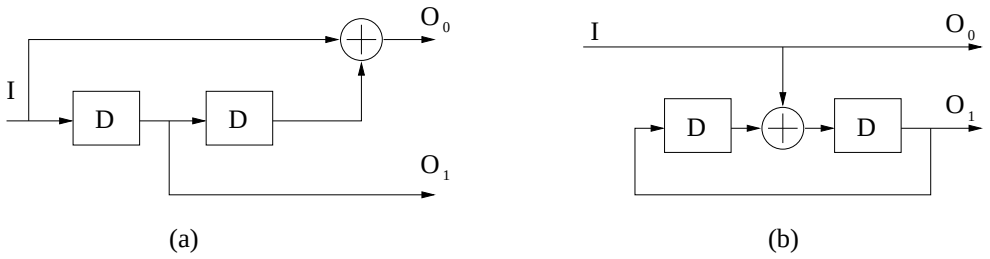

Fig. 2. Examples of 4-state convolutional codes used for TCQ (a) Non-systematic form; (b) Systematic form.

The trellises used in TCQ are usually based on a underlying convolutional code. Examples of convolutional codes with four states and their state transition diagrams are shown in Figure 2 and Figure 3, respectively. The non-systematic convolutional

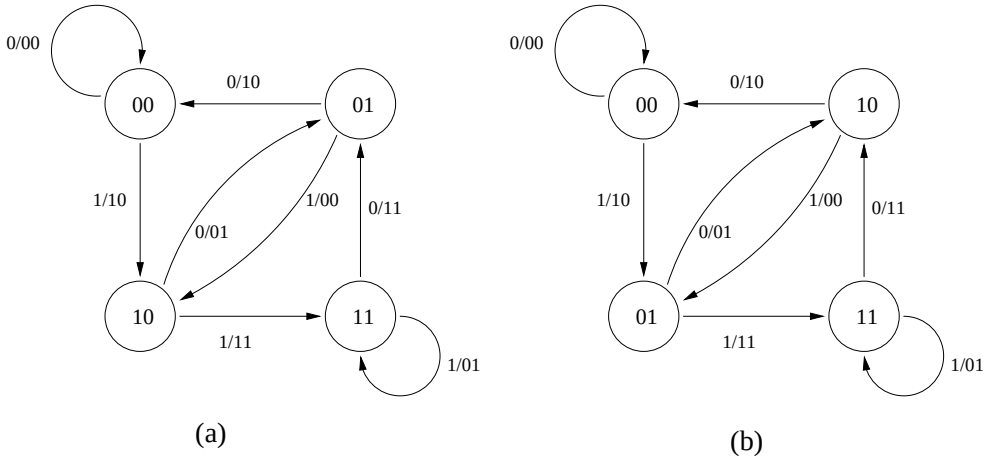

Fig. 3. State transition diagrams for the 4-state convolutional codes in (a) Figure 2(a) (b) Figure 2(b).

code in Figure 3(a) corresponds to the parity check matrix $H_{non} = [1+D^2 \;\; D]$, and the systematic one in Figure 3(b) corresponds to the parity check matrix $H_{sys} = [1 \;\; \frac{D}{1+D^2}]$. Although the block diagrams of the two are different, both codes generate the same set of output sequences, hence they are essentially identical for TCQ. In the sequel, we always focus on the rate-$\frac{1}{2}$ systematic convolutional codes because only the last bit plane of the output sequences has memory in the systematic case. This is a very desirable property when the output sequence is to be compressed.

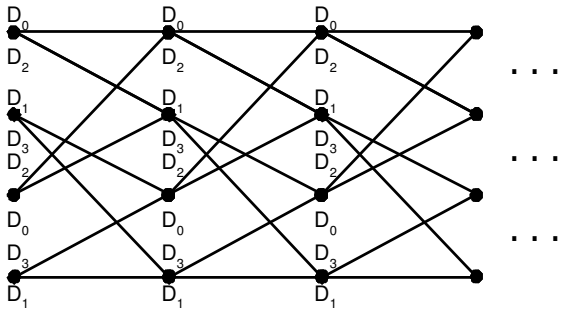

Fig. 4. An example of a multi-stage trellis.

Based on a size-2^{R+1} codebook and a rate-$\frac{1}{2}$ N-state trellis, we can quantize the source X using the *Viterbi* algorithm. For a length-n block of source samples $X^n = \{X_0, X_1, \ldots, X_{n-1}\}$, n stages of the N-state trellis are employed. Then we have $n+1$ columns of states which are connected by trellis transitions. For each state, there are exactly two transitions to and from it. Each transition is assigned with a coset $D_i, i = 0, 1, 2, 3$ where i is the 2-bit output message corresponding to the transition. An example of a multi-stage trellis is shown in Figure 4. Note that the two transitions entering or leaving a state correspond to the two cosets of the same superset (e.g., D_0 and D_2 are the two cosets for transitions leaving state-0, while D_1 and D_3 are the two cosets for transitions entering state-2). Hence only a half of the 2^{R+1} codewords are possible at each stage, and R bits are needed to represent these 2^R possible codewords for each source sample. Speaking at block level, there are 2^{nR} code vectors available for a source vector X^n, and the *Viterbi algorithm* targets at finding the code vector that is nearest to the source vector in the sense of minimizing the MSE. The algorithm is given by:

The Viterbi Algorithm for Trellis Coded Quantization

1. Given a source vector $X^n = \{X_0, X_1, \ldots, X_{n-1}\}$, initialize distortions for all the states in stage -1 as $d_0^{-1} = 0.0$, $d_1^{-1} = d_2^{-1} = \ldots = d_{N-1}^{-1} = \infty$, where superscript 0 is the stage number, and subscripts are the state number. Let $i = 0$.

2. For each state j $(0 \leq j \leq N-1)$ at stage i, find the two trellis transitions entering it. Let $(S(j,0), S(j,1))$ denote the two starting states of the transitions, and $(O(j,0), O(j,1))$ denote the corresponding outputs. Then find the codeword in coset $D_{O(j,0)}$ that is nearest to the source sample X_i. Suppose $q_{O(j,0)}^{k_{i,0}}$ is the nearest one with distortion $d_0 = (q_{O(j,0)}^{k_{i,0}} - X_i)^2$. Similarly, we find $q_{O(j,1)}^{k_{i,1}}$ with smallest distortion $d_1 = (q_{O(j,1)}^{k_{i,1}} - X_i)^2$.

3. Compare the two cumulate distortion $d^{i-1}_{S(j,0)}+d_0$ and $d^{i-1}_{S(j,1)}+d_1$, set the new cumulate distortion to $d^i_j = \min\{d^{i-1}_{S(j,0)}+d_0, d^{i-1}_{S(j,1)}+d_1\}$, and delete the transition corresponds to the larger distortion.

4. After all the cumulate distortions $d^i_j, 0 \le j \le N-1$ are found, set $i = i+1$. If $i < n-1$, goto step 2, otherwise, proceed to step 5.

5. Find the final state S_{final} with the smallest cumulate distortion $d^{n-1}_{S_{final}}$ among $d^{n-1}_j, 0 \le j \le N-1$, and trace back from S_{final} to the starting state to find the corresponding trellis path that produces $d^{n-1}_{S_{final}}$. Hence the length-n code vector that produces $d^{n-1}_{S_{final}}$ is also known.

6. For the i-th codeword $q^{k_i}_{C_i}$ in the selected code vector, output k_i using $R-1$ bits, and then output the higher bit of C_i. Do this for each i, $0 \le i \le n-1$.

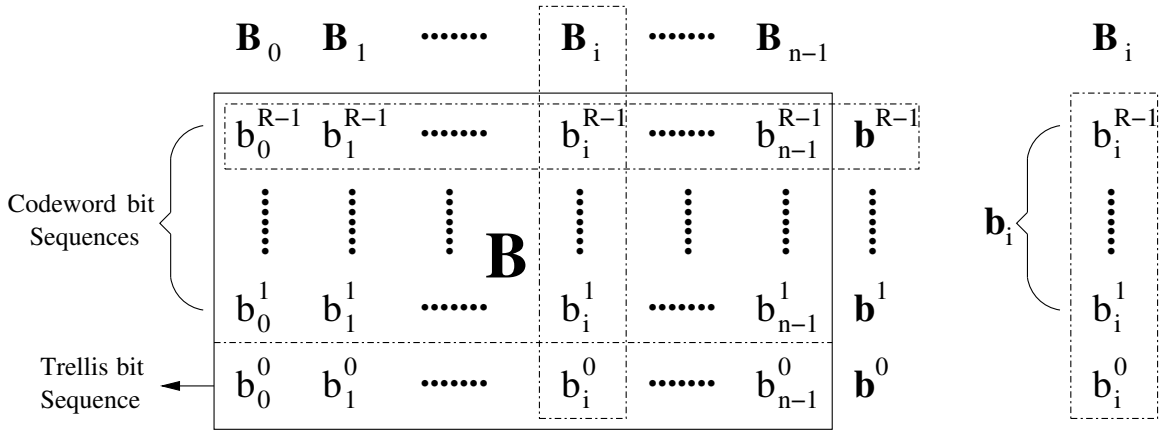

Fig. 5. Rate-R TCQ index matrix for block length n.

To index the code vector found by the Viterbi algorithm, an $R \times n$ index matrix, denoted as $\mathbf{B}$, is needed. The R bits for the i-th sample are called the i-th *TCQ index* and are denoted as $B_i = \{b^{R-1}_i, \ldots, b^1_i, b^0_i\}$. The last bit b^0_i is called the i-th *trellis bit*

which specifies the surviving trellis transition (thus the corresponding coset index C_i) between stage-$(i-1)$ and stage-i. The other $R-1$ bits $\mathbf{b}_i = \{b_i^{R-1}, \ldots, b_i^1\}$ are called *codeword bits* and they specify the nearest codeword in coset D_{C_i} that is closest to the source sample X_i. The length-n trellis bit sequences is denoted as $\mathbf{b}^0$, and the other $R-1$ codeword bit sequences are written as $\mathbf{b}^1, \ldots, \mathbf{b}^{R-1}$. Figure 5 shows a rate-$R$ TCQ index matrix for a block of n input samples.

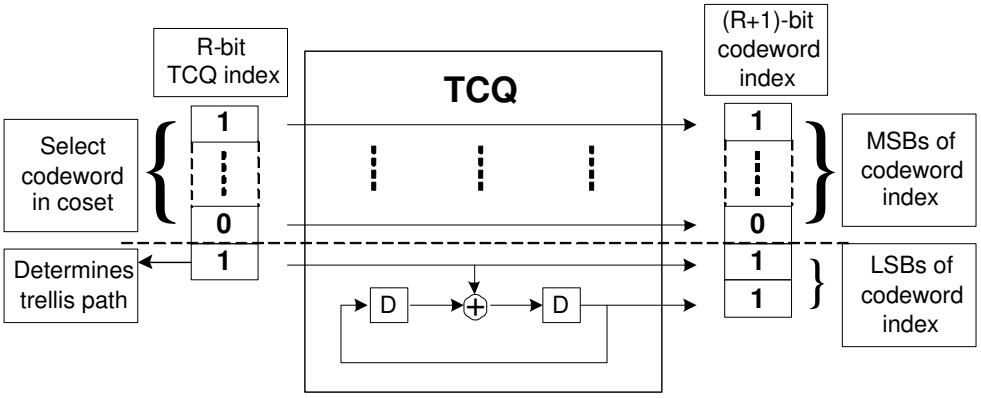

Fig. 6. The quantization procedure of rate-R TCQ.

The quantization procedure is illustrated in Figure 6, and a simple example is given as follows:

Example Let TCQ rate $R = 2$, block length $n = 4$. The codebook consists of eight codewords $\{-7, -5, -3, -1, 1, 3, 5, 7\}$ which are divided into four cosets $D_0 = \{-7, 1\}$, $D_1 = \{-5, 3\}$, $D_2 = \{-3, 5\}$, and $D_3 = \{-1, 7\}$. We use the 4-state trellis in Figure 2(b). Suppose the source samples are $X^4 = \{-4.1, 2.2, 0.3, -2.5\}$, we apply the Viterbi algorithm on X^4, as shown in Figure 7. We skip the details and directly come to the final quantization output given by a 2×4 TCQ index matrix

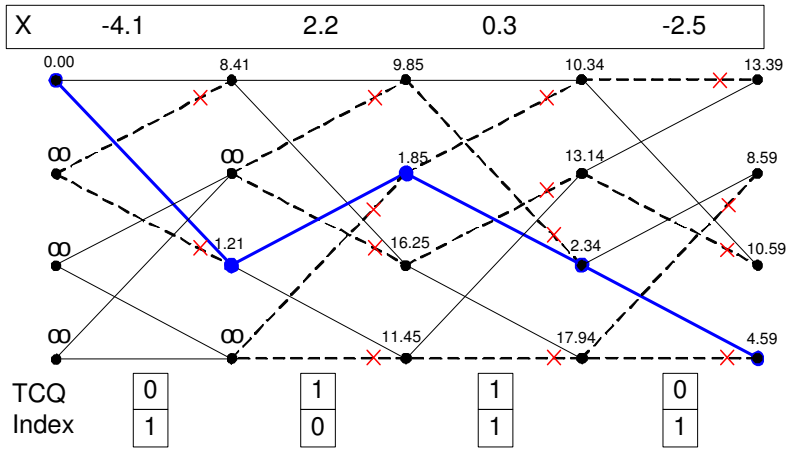

Fig. 7. The quantization of source block $X^4 = \{-4.1, 2.2, 0.3, -2.5\}$.

$$\mathbf{B} = \left\{ \begin{array}{cccc} 0 & 1 & 1 & 0 \\ 1 & 0 & 1 & 1 \end{array} \right\}.$$

The performance of fixed rate TCQ with a 256-state trellis is about 0.2 dB away from the distortion-rate bound for uniform sources, which is better than any vector quantizer of dimension less than 69 [31]. However, the performance gap becomes more than 0.5 dB for Gaussian sources. This larger gap can be further reduced by entropy coding.

2. Entropy-Coded TCQ (ECTCQ)

When quantizing non-uniform sources using R-bit TCQ, the entropy rate of the output TCQ index sequence is always less than the TCQ rate R. This is the motivation for adding an entropy coding component after TCQ. However, the TCQ index sequence is of memory, thus cannot be compressed directly using Huffman coding or arithmetic coding. Three approaches are introduced in [33] to explore the memory in the TCQ index sequence and compute the encoding rate after entropy coding.

1. *Coset entropy (subset entropy).*

   Directly transmit the trellis bit sequence using one bit/sample. Then the decoder knows exactly the trellis path (thus the coset index C_i for each $0 \leq i \leq n-1$) with which the source vector X^n is quantized. Given the trellis path, the $R-1$ bit/sample codeword bit sequence are memoryless. Then the average encoding rate can be expressed as $H(Q(X)|C)+1$, where $Q(X)$ is the quantized version of the source X, i.e., $Q(X) = q_i^j$ for some $0 \leq i \leq 3$ and $0 \leq j \leq 2^{R-1}-1$; C is the random variable characterizing the coset indices C_i's. By definition, we have

$$\begin{aligned} & H(Q(X)|C) \\ = & -\sum_{i=0}^{3} P(Q(X) \in D_i) \cdot \\ & \sum_{j=0}^{2^{R-1}-1} P(Q(X) = q_i^j | Q(X) \in D_i) \cdot \log_2 P(Q(X) = q_i^j | Q(X) \in D_i). \end{aligned} \quad (2.2)$$

   Using the coset entropy approach to compress the TCQ index sequence is intuitive and easy to implement. However, the encoding rate is always larger than one bit/sample, which is very inefficient at low rate.

2. *State entropy*

   In the Viterbi algorithm for TCQ, given the current state and the selected codeword, we know the coset index of the codeword, i.e., the output from current state to next state, hence the next state is uniquely determined. Note that from one state S, only half of the codewords are available to select, they are from the same superset B_0 or B_1. Let the 2^R codewords available for state S be $\{q_{S,0}^*, q_{S,1}^*, \ldots, q_{S,2^R-1}^*\}$, then the encoding rate can be expressed as

$$H(Q(X)|S)$$

$$= -\sum_{s=0}^{N-1} P(S=s) \cdot \sum_{j=0}^{2^R-1} P(Q(X)=q^*_{s,j}|S=s) \cdot \log_2 P(Q(X)=q^*_{s,j}|S=s). \quad (2.3)$$

The encoder designs N entropy codebooks for all the N states, and compresses the i-th codeword index using the s-th entropy codebook where s is the current state. At the decoder side, we know the starting state $S_{-1} = 0$, then the first codeword index can be decoded using the entropy codebook designed for state S_{-1}. Given this codeword index and the starting state $S_{-1} = 0$, the second state S_0 can be found. Again, the second codeword index is decoded using the entropy codebook designed for state S_0. Proceeding in this way, all the codeword indices can be decoded losslessly.

3. *Superset entropy*

Similar to the state entropy approach, because from one state S, only the codewords from one superset of (B_0, B_1) are available, hence the encoding rate can be expressed as (recall that $B_0 = D_0 \cup D_2$, $B_1 = D_1 \cup D_3$)

$$H(Q(X)|B) = -\sum_{i=0}^{1} P(Q(X) \in B_i) \cdot \sum_{j=0}^{2^{R-1}-1} \sum_{k=0}^{1} P(Q(X)=q^j_{i+2k}|Q(X)\in B_i) \cdot \log_2 P(Q(X)=q^j_{i+2k}|Q(X)\in B_i). \quad (2.4)$$

In this approach, the encoder designs two entropy codebooks for B_0 and B_1, and compresses each codeword index using the entropy codebook designed for the corresponding superset. The decoding procedure is similar to (2). Because given the current state, we know in which superset will the selected codeword be; with this information, we can uniquely decode the codeword index; and the

next state can be determined from the current state and the codeword index. Hence, lossless decoding is ensured.

It is stated in [31] that "256-state entropy-coded TCQ can achieve MSE performance within about 0.2 dB of the distortion-rate function at all rate R for any smooth PDF," and "uniform thresholds with centriod codewords are very near optimal." We also implement the ECTCQ scheme using both coset entropy approach and superset entropy approach, and the simulation results verify the conclusions on ECTCQ in [31].

C. Low Density Parity Check (LDPC) Codes

Low Density Parity Check (LDPC) codes are linear block codes with a "low-density" parity check matrix in the sense that the number of non-zero elements in the parity matrix is relatively small. If the parity check matrix satisfies

1. each column has j 1's (normally $j \geq 3$ to produce good performance), and
2. each row has $k(> j)$ 1's,

the corresponding code is referred to as *regular LDPC code*; if the numbers of 1's in the rows (or the columns) of the parity check matrix are not all equal, we have *irregular LDPC code*.

A LDPC code can be represented using a Tanner graph. As an example, the Tanner graph for a binary $(6, 2)$-LDPC code is shown in Figure 8, the corresponding

parity check matrix H is

$$H = \begin{bmatrix} 1 & 0 & 1 & 1 & 0 & 0 \\ 1 & 1 & 0 & 0 & 0 & 1 \\ 0 & 0 & 1 & 0 & 1 & 0 \\ 0 & 0 & 0 & 1 & 1 & 1 \end{bmatrix} \tag{2.5}$$

Each circle at the left side of the graph is called a *bit node* which corresponds to a column of the parity check matrix; each square at the right side of the graph is called a *check node* which corresponds to a row of the parity check matrix. There exists a connection between the i-th bit node and the j-th check nod only if the intersecting entry of the i-th column and the j-th row of the parity check matrix is a one, and each of these connections is called an *edge*. The *degree* of a node (bit or check) is defined by the number of edges that are connected to it, while the left (right) degree of an edge is the degree of the bit (check) nod that it connects.

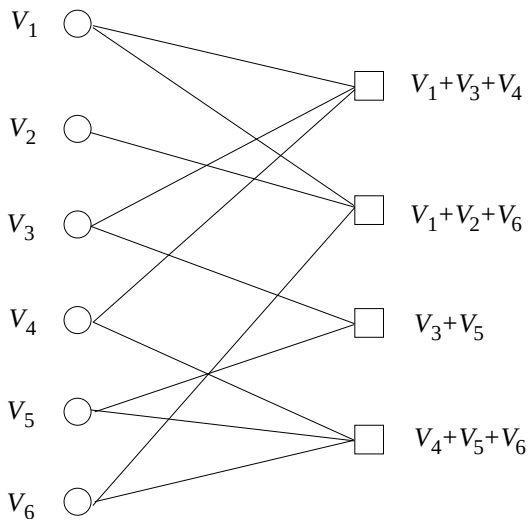

Fig. 8. The Tanner graph of a binary (6,2)-LDPC code.

The *degree profile* (λ, ρ) of a LDPC code is defined by the sequence generating functions $\lambda(x) = \sum_{i=2}^{d_{l_{max}}} \lambda_i x^{i-1}$ and $\rho(x) = \sum_{i=2}^{d_{r_{max}}} \rho_i x^{i-1}$ where λ_i is the fraction of edges with left degree i and ρ_i is the fraction of edges with right degree i; $d_{l_{max}}$ and $d_{r_{max}}$ are the maximum left degree and the maximum right degree of all the edges. The rate of the code is then given by $1 - \frac{\int \rho(x)}{\int \lambda(x)}$. For regular LDPC codes, $\lambda(x) = x^{i-1}$ and $\rho(x) = x^{j-1}$.

The encoding of LDPC codes is the classical encoding of linear block code, while message-passing algorithm is employed in the decoding of LDPC codes. As the name suggested, messages are exchanged between two ends of each branch in a message-passing algorithm. The message going into or out of a variable node possesses the "belief" of the value of that variable node. For binary LDPC codes, these messages are typically in the form of log-likelihood ratios (i.e., $\log \frac{p(\text{observation}|V_i=1)}{p(\text{observation}|V_i=0)}$ for the messages passing into or out of the variable node V_i). Upon receiving the messages, both variable and check nodes update the messages by combining the beliefs of the messages, and send the new messages to the other ends. To avoid the belief in a message is doubly counted, the message originated from the same branch is not included in the update. The detailed algorithm is described in [34].

Given that the channel satisfies certain symmetry condition, the performance of the LDPC code is independent of the input codeword to be transmitted. Hence, we can assume any codeword to be sent when we analyze the LDPC code performance. In specific, by assuming all-one codeword is sent and by tracking the density distribution of the average beliefs of the variable nodes, we could estimate the probability of decoding error after any number of iterations in theory. However, this cannot be easily done for a specific LDPC code since each variable/check node can have different degree. Nonetheless, if we consider an ensemble of codes which bear the same degree profile in the sense that the fraction of nodes with any particular degree is

the same, then the problem become tractable and this technique is commonly known as density evolution. Density evolution can be employed for LDPC code design [35]. The basic idea is to adjust the degree profile interactively such that the decoding error probability predicted by density evolution is smallest.

CHAPTER III

WYNER-ZIV CODING BASED ON TCQ AND LDPC CODES

In this chapter, we consider TCQ and LDPC codes for the quadratic Gaussian Wyner-Ziv problem. The main idea is to quantize the source input X using TCQ, and then employ LDPC codes to implement Slepian-Wolf coding of the quantized source input $Q(X)$ given the side information Y at the decoder. Assuming ideal Slepian-Wolf coding in the sense of achieving the theoretical limit $H(Q(X)|Y)$, it will be shown that Slepian-Wolf coded TCQ (SWC-TCQ) performs 0.2 dB away from the Wyner-Ziv distortion-rate function $D^*_{WZ}(R)$ at high rate. This result mirrors that of entropy-coded TCQ in classic source coding and establishes the connection between performances of high-rate Wyner-Ziv coding and classic source coding. Practical designs with TCQ, irregular LDPC code (for Slepian-Wolf coding) and optimal estimation at the decoder perform 0.82 dB away from $D^*_{WZ}(R)$ at medium bit rates (e.g., ≥ 1.5 b/s). With 2-D tellis coded vector quantization, the performance gap to $D^*_{WZ}(R)$ is only 0.66 dB at 1.0 b/s and 0.47 dB at 3.3 b/s.

The organization is as follows. In Section A, we describe the Wyner-Ziv coding problem and the Wyner-Ziv limit for the general case and for the quadratic Gaussian case; the general framework of Slepian-Wolf coded quantization for Wyner-Ziv coding is also discussed briefly. Then in Section B, the proposed SWC-TCQ scheme will be presented in details. Section C focuses on the exploration of statistical properties of the input-output pairs for TCQ and two-dimensional TCVQ. These statistics are used in the decoding algorithms for the codeword bits that are given in Section D. An optimal estimation algorithm is then presented in Section E. Simulation results with TCQ and 2-D TCVQ are shown in Section F, with the conclusions drawn in Section G.

A. Wyner-Ziv Coding

Wyner-Ziv coding [2] refers to lossy source coding with side information at the decoder.

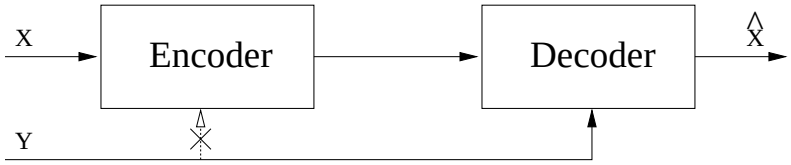

Fig. 9. Wyner-Ziv coding (source coding with side information at the decoder).

As illustrated in figure 9, the source X is to be compressed using rate R and decompressed at the decoder with Y as side information. The reconstructed source $\hat{X}$ satisfies a distortion constraint

$$E\{\frac{1}{n}\sum_{i=0}^{n-1} d(X_i, \hat{X}_i)\} = E\{d(X, \hat{X})\} \leq D, \tag{3.1}$$

for a given target distortion $D \geq 0$. The goal is to minimize the transmission rate R. The general Wyner-Ziv rate-distortion function is given by [2]

$$R^*_{WZ}(D) = \inf_{Y \to X \to Z; E\{d(X,\hat{X}(Z,Y))\} \leq D} I(X; Z|Y), \tag{3.2}$$

where Z is an auxiliary random variable and $\hat{X}(Z, Y)$ is the decoding function.

Recall the classical rate-distortion function defined by

$$R_X(D) = \inf_{E\{d(X,U)\} \leq D} I(X; U), \tag{3.3}$$

where U is an auxiliary random variable that satisfies the distortion constraint. Hence the rate-distortion function of coding X given Y at both the encoder and the decoder

can be expressed as

$$R_{X|Y}(D) = \inf_{E\{d(X,U)\}\leq D} I(X;U|Y). \tag{3.4}$$

In general, there is a rate loss with Wyner-Ziv coding, i.e., $R^*_{WZ}(D) > R_{X|Y}(D)$ in most cases. This loss is up to 0.22 bit for binary sources with Hamming distance and less than 0.5 bit/sample for continuous sources with MSE measure.

However, for jointly Gaussian sources with MSE distortion measure, Wyner-Ziv coding suffers no loss due to the unavailability of the side information at the encoder. Let X and Y be jointly Gaussian sources with covariance matrix

$$\Lambda = \begin{pmatrix} \sigma_x^2 & \rho\sigma_x\sigma_y \\ \rho\sigma_x\sigma_y & \sigma_y^2 \end{pmatrix}. \tag{3.5}$$

Then the Wyner-Ziv limit $R^*_{WZ}(D)$ can be shown to be equal to $R_{X|Y}(D)$, and

$$R^*_{WZ}(D) = R_{X|Y}(D) = \frac{1}{2}\log^+ \frac{(1-\rho^2)\sigma_x^2}{D}, \tag{3.6}$$

where $\log^* x = \max\{\log x, 0\}$.

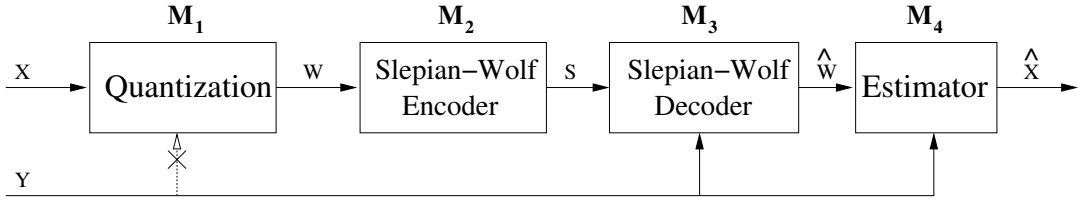

Fig. 10. The general Slepian-Wolf coded quantization framework for Wyner-Ziv coding).

The general Slepian-Wolf coded quantization framework for Wyner-Ziv coding is shown in Figure 10. The quantization part is a mapping

$$M_1 : \mathcal{R}^n \to \{1, 2, \ldots, 2^{nR_s}\}, \tag{3.7}$$

where R_s is the the source coding rate. M_1 partitions the source space $\mathcal{R}^n$ into 2^{nRs} disjoint regions $\mathcal{V} = \{V_1, V_2, \ldots, V_{2^{nRs}}\}$. We refer to the region V_i to which X^n is quantized as *active region*. The Slepian-Wolf encoder is a mapping

$$M_2 : \{1, 2, \ldots, 2^{nR_s}\} \rightarrow \{1, 2, \ldots, 2^{nR}\}, \tag{3.8}$$

where R is the the transmission rate. M_2 aims at finding the index of the coset of the channel code containing the index of the active region. This coset index is often referred to as *Syndrome*. Hence a source code with 2^{nR_s} indices is partitioned into 2^{nR} cosets of a certain channel code which has a total number of code words $2^{nR_c} = 2^{nR_s}/2^{nR} = 2^{n(Rs-R)}$. The Slepian-Wolf decoder is a mapping

$$M_3 : \mathcal{R}^n \times \{1, 2, \ldots, 2^{nR}\} \rightarrow \{1, 2, \ldots, 2^{nR_s}\}, \tag{3.9}$$

which recovers the index of the active region in the specified coset by finding the most likely region given the side information Y. The estimator is a mapping

$$M_4 : \mathcal{R}^n \times \{1, 2, \ldots, 2^{nR_s}\} \rightarrow \mathcal{R}^n, \tag{3.10}$$

which finds the best estimate of X^n given the side information and the active region V_i containing X^n. For MSE distortion measure, this best estimate is the conditional mean $E\{X^n | Y^n, X^n \in V_i\}$. Finally, the reconstructed source $\hat{X}^n$ can be expressed as

$$\hat{X}^n = M_4 \left\{ Y^n, M_3\{Y^n, M_2[M_1(X^n)]\} \right\}. \tag{3.11}$$

B. Proposed SWC-TCQ Scheme

Assume $X = Y + Z$ where $Y \sim N(0, \sigma_Y^2)$ and $Z \sim N(0, \sigma_Z^2)$ are independent. For a target bit rate, we aim to minimize $E[d(X, \hat{X})]$. Our proposed SWC-TCQ scheme is shown in Figure 11. The input X is grouped into blocks of length 1000 samples

before going through an R-bit TCQ [4] in the *TCQ Encoder*, which employs a standard Viterbi encoder and a uniform-threshold quantizer. The quantizer encoder has 2^{R+1} uniformly spaced codewords, which are partitioned into four cosets, each having 2^{R-1} codewords. Using the same notation as in chapter II(B), the R-bit TCQ index sequence $\mathbf{B}$ consists of one trellis bit sequence $\mathbf{b}^0$ and $R-1$ codeword bit sequences $\{\mathbf{b}^1, \mathbf{b}^2, \cdots, \mathbf{b}^{R-1}\}$. Denote the i-th TCQ index as $\mathbf{B}_i$, then $\mathbf{B}_i$ consists of a trellis bit b_i^0 and an $(R-1)$-bit codeword $\mathbf{b}_i = \{b_i^1, b_i^2, \cdots, b_i^{R-1}\}$, i.e., $\mathbf{B}_i = \{b_i^0, \mathbf{b}_i\} = \{b_i^0, b_i^1, \cdots, b_i^{R-1}\}$. The *Syndrome Encoder* compresses $\mathbf{B} = \{\mathbf{b}^0, \mathbf{b}^1, \cdots, \mathbf{b}^{R-1}\}$ into R syndrome sequences $\mathbf{S} = \{\mathbf{s}^0, \mathbf{s}^1, \cdots, \mathbf{s}^{R-1}\}$ using R LDPC code based Slepian-Wolf codes of different rates [14]. We assume that $\mathbf{S}$ is revealed to the decoder via a noiseless channel.

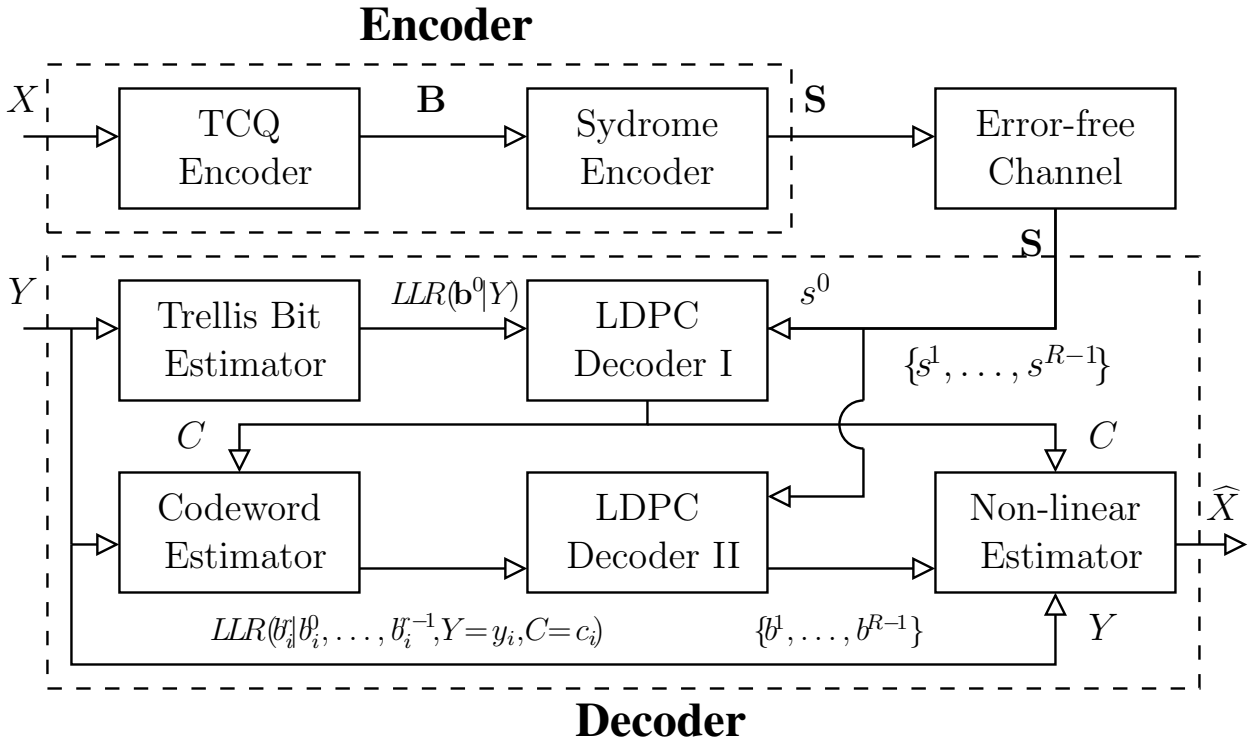

Fig. 11. Block diagram of the SWC-TCQ scheme.

At the decoder, the side information Y is fed into the *Trellis Bit Estimator* and *Codeword Estimator* to compute the log-likelihood ratios (LLRs) of the trellis bits $\mathbf{b}^0$ and codeword $\mathbf{b_i}$ given Y, respectively.

Since the trellis bits in $\mathbf{b}^0$ have memory and they exactly determine the trellis path, computations in the *Trellis Bit Estimator* are carried out block by block. This is done by randomly generating realizations of $Z \sim N(0, \sigma_Z^2)$, quantizing $Y + Z$ with the same TCQ used in the encoder, and counting the number of 0's and 1's in $\mathbf{b}^0$ to obtain $LLR(\mathbf{b}^0|Y)$. *LDPC Decoder I* runs the message-passing algorithm based on $LLR(\mathbf{b}^0|Y)$ and the syndrome sequence $\mathbf{s}^0$ to reconstruct $\mathbf{b}^0$. Although our estimation of $LLR(\mathbf{b}^0|Y)$ might not be optimal, experiments show that *LDPC Decoder I* performs reasonably well except at low rate for the conditional entropy $H(\mathbf{b}^0|Y)$ approaches one as R increases. With enough rate for $\mathbf{s}^0$, it is reasonable to assume that $\mathbf{b}^0$ is recovered error free when decoding $\{\mathbf{b}^1, \mathbf{b}^2, \cdots, \mathbf{b}^{R-1}\}$ or the $\mathbf{b}_i$'s.

To avoid the compression inefficiency of $\mathbf{b}^0$ due to the suboptimality in estimating $LLR(\mathbf{b}^0|Y)$, we employ 2-D TCVQ to make the rate of $\mathbf{b}^0$ fractional when the target bit rate is low (e.g., one b/s). In this case, $\mathbf{b}^0$ is directly transmitted without compression.

With $\hat{\mathbf{b}}^0$ available at the decoder, the coset index sequence C of all samples is known. Thus operation of the *Codeword Estimator* can be sample based instead of block based. In Section C, we will look deeper into TCQ, extract key information from it, and combine it with the side information Y at the decoder. Based on that, we will devise in Section D a novel way of computing $LLR(b_i^r|\hat{b}_i^0, \cdots, \hat{b}_i^{r-1}, Y = y_i, C = c_i)$ for $1 \leq r \leq R-1$. Using this LLR, *LDPC Decoder II* sequentially decodes $b_i^1, b_i^2, \cdots, b_i^{R-1}$ with the help of transmitted syndrome sequences $\mathbf{s}^1, \mathbf{s}^2, \cdots, \mathbf{s}^{R-1}$.

Finally, the *Nonlinear Estimator* reconstructs $\hat{X}$ based on both $\{\hat{\mathbf{b}}^0, \hat{\mathbf{b}}^1, \cdots, \hat{\mathbf{b}}^{R-1}\}$ and Y at the decoder. The estimation algorithm used in [11, 12] is linear, which is

good only when the quantization error $Q(X) - X$ and Z are independent Gaussian random variables [7]. We know, however, that $Q(X) - X$ is not Gaussian unless $Q(X)$ is optimal in the sense that the resulting source code approaches the rate-distortion performance. This is because the Gaussian source is the hardest to compress. Thus, although TCQ is an efficient quantization technique, $Q(X) - X$ is not Gaussian, especially at low rate. Using results developed in Section C again, we describe a powerful and universal method of performing optimal estimation in Section E.

C. Statistics of TCQ/TCVQ Indices

1. Statistics of TCQ Indices

TCQ [4] is the source coding counterpart of TCM [30]. It can be thought of as being a type of vector quantization because of the expanded signal set it uses. Since we are concerned with SWC-TCQ, ECTCQ is more relevant to us. It is stated in [31] that for ECTCQ, uniform thresholds with centroid codewords at the decoder are near optimal. This leads us to the uniform-threshold quantizer. Let the quantized version of the input sample x_i be $q_{c_i}^{\mathbf{b}_i}$, where $c_i \in \{0, 1, 2, 3\}$ is the coset index. Fig. 12 shows the eight codewords of the quantizer *encoder* for a 2-bit TCQ.

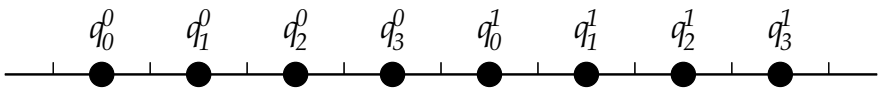

Fig. 12. A uniform-threshold quantizer with 8 codewords for a 2-bit TCQ.

It is a challenging task to achieve good Wyner-Ziv coding performance at low rate because as the rate becomes scarce, it is imperative to explore the memory in the trellis indices for compression and to perform optimal estimation at the joint decoder.

Toward this end, we first look into $P(Q(X) = q_c^{\mathbf{b}}|X)$: the conditional probability that X is quantized to $q_c^{\mathbf{b}}$ given the source X. This conditional probability builds a connection between the input and output of TCQ, and characterizes the behavior of the quantization procedure. To compute $P(Q(X) = q_c^{\mathbf{b}}|X)$, we first partition the granular region of our uniform-threshold quantizer into N length-δ mini-cells, $\Delta_1, \Delta_2, \ldots, \Delta_N$, and denote w_n as the mid-point of Δ_n for $1 \leq n \leq N$. The partition is illustrated in Figure 13. Then the conditional probability $P(Q(X) = q_c^{\mathbf{b}}|X)$ can be approximated by $P(Q(X) = q_c^{\mathbf{b}}|X \in \Delta_n)$ as N goes to infinity, where Δ_n is the mini-cell containing X.

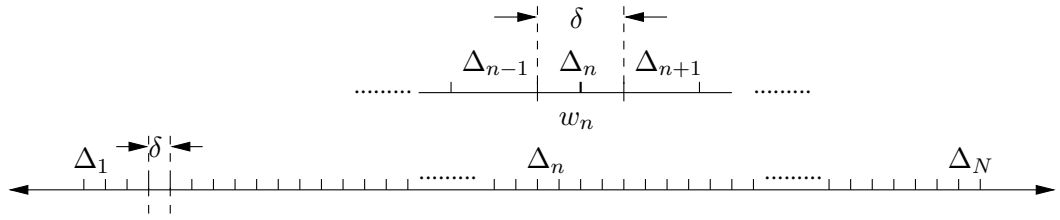

Fig. 13. Discretization of the granular region.

To compute the desired probability, a large number of simulations are run for TCQ on the training data $X \sim N(0, \sigma_X^2)$. We count the number of occurrences for each possible input-output pair $\{(n, q_c^{\mathbf{b}}) : X \in \Delta_n, Q(X) = q_c^{\mathbf{b}}\}$. Recall that at each stage in the Viterbi algorithm of TCQ, for a given source sample $X = x$, only four codewords are possible for $Q(x)$, which are the nearest codewords to x in each of the four cosets. In other words, given $X \in \Delta_n$ and $Q(X) \in D_c, c = 0, 1, 2, 3$, $Q(X)$ must be the codeword in D_c that is closest to w_n, the mid-point of Δ_n (assume δ is very small). We denote this codeword given $X \in \Delta_n$ and $Q(X) \in D_c$ as $q_c^{\mathbf{b}(n,c)}$. Hence, we only need to count the number of occurrences for each pair $\{(n, c) : X \in \Delta_n, Q(X) \in D_c\}$. Let $count(n, c)$ be the number of occurrences correspond to pair (n, c), then the

desired probability becomes

$$\begin{aligned} & P(Q(X) = q_c^{\mathbf{b}(n,c)} | X \in \Delta_n) \\ = & \frac{P(Q(X) = q_c^{\mathbf{b}(n,c)}, X \in \Delta_n)}{P(X \in \Delta_n)} \\ = & \frac{P(Q(X) \in D_c, X \in \Delta_n)}{\sum_{c'=0}^{3} P(Q(X) \in D_{c'}, X \in \Delta_n)} \\ \approx & \frac{count(n,c)}{\sum_{c'=0}^{3} count(n,c')}, \end{aligned} \tag{3.12}$$

and for other $\mathbf{b} \neq \mathbf{b}(n,c)$, $P(Q(X) = q_c^{\mathbf{b}} | X \in \Delta_n) = 0$. Hence the conditional probability $P(Q(X) = q_c^{\mathbf{b}} | X \in \Delta_n)$ is available for all $q_c^{\mathbf{b}}$ and n.

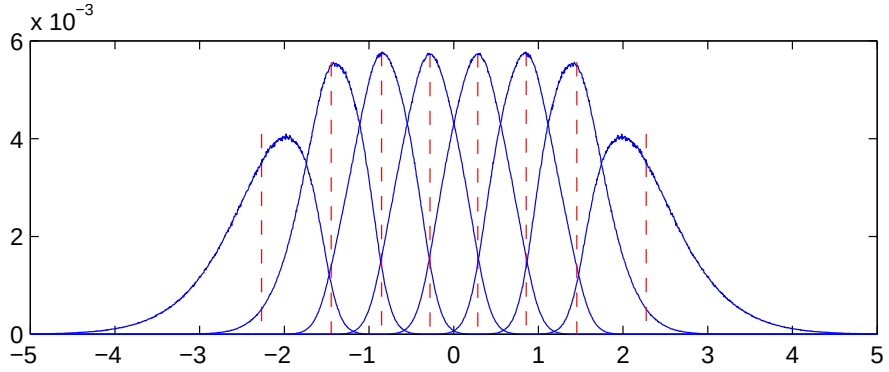

Fig. 14. $f(X|Q(X) = q_{c_i}^{\mathbf{b}_i})$ generated with the 2-bit TCQ shown in Fig. 12 with $q = 0.575$ and $\sigma_X^2 = 1.28$. Dashed lines mark the centroids used in the quantizer decoder.

We can also compute the conditional PDF $f(X|Q(X) = q_c^{\mathbf{b}})$ based on the numbers $\{count(n,c), 1 \leq n \leq N, 0 \leq c \leq 3\}$, because this conditional PDF can be approximated by $P(X \in \Delta_n | Q(X) = q_c^{\mathbf{b}})$, which is computed using

$$\begin{aligned} & P(X \in \Delta_n | Q(X) = q_c^{\mathbf{b}(n,c)}) \\ = & \frac{P(Q(X) = q_c^{\mathbf{b}(n,c)}, X \in \Delta_n)}{P(Q(X) = q_c^{\mathbf{b}})} \end{aligned}$$

$$
\begin{aligned}
&= \frac{P(Q(X) \in D_c, X \in \Delta_n)}{\sum_{n'=1}^{N} P(Q(X) \in D_c, X \in \Delta_{n'})} \\
&\approx \frac{count(n,c)}{\sum_{n'=1}^{N} count(n',c)},
\end{aligned} \tag{3.13}
$$

and $P(X \in \Delta_n | Q(X) = q_c^{\mathbf{b}}) = 0$ for other $\mathbf{b} \neq \mathbf{b}(n,c)$. From Figure 14, we clearly observe the non-Gaussian shape of $f(X|Q(X) = q_c^{\mathbf{b}})$ for limitary cells of a 2-bit TCQ. Note that the values of the conditional probability $P(Q(X) = q_c^{\mathbf{b}} | X \in \Delta_n)$ for each $\{1 \leq n \leq N, 0 \leq c \leq 3\}$ can be shared by both the encoder and the decoder using a look-up table.

2. Statistics of TCVQ Indices

To avoid the compression inefficiency of the trellis bit sequence $\mathbf{b}^0$ due to the suboptimality in estimating $P(\mathbf{b}^0|Y)$, we employ TCVQ to make the rate (in b/s) of the trellis bit fractional (e.g., for two-dimensional TCVQ, the rate of the trellis bit is 0.5 b/s) when the target bit rate is low (e.g., one b/s). In this case, $\mathbf{b}^0$ is directly transmitted without compression. However, the encoding-decoding complexity of such a TCVQ based scheme will be significantly higher than the SWC-TCQ scheme. Hence we need to reduce this coding complexity by exploring the symmetric properties among the four cosets.

For a rate-$(R + \frac{1}{2})$ 2-D TCVQ, to quantize a length-n source block X^n, every two source samples are grouped together as a 2-D source vector, and the resulting $\frac{n}{2}$ source vectors form a length-$\frac{n}{2}$ block of source vectors. We denote such a block as

$$
\vec{X}^{\frac{n}{2}} = \{\vec{X}_0, \vec{X}_1, \ldots, \vec{X}_{\frac{n}{2}-1}\} = \left\{ \begin{pmatrix} X_1 \\ X_0 \end{pmatrix}, \begin{pmatrix} X_3 \\ X_2 \end{pmatrix}, \ldots, \begin{pmatrix} X_{n-1} \\ X_{n-2} \end{pmatrix} \right\}. \tag{3.14}
$$

Then we construct a two-dimensional codebook with 2^{R+1} codewords in each

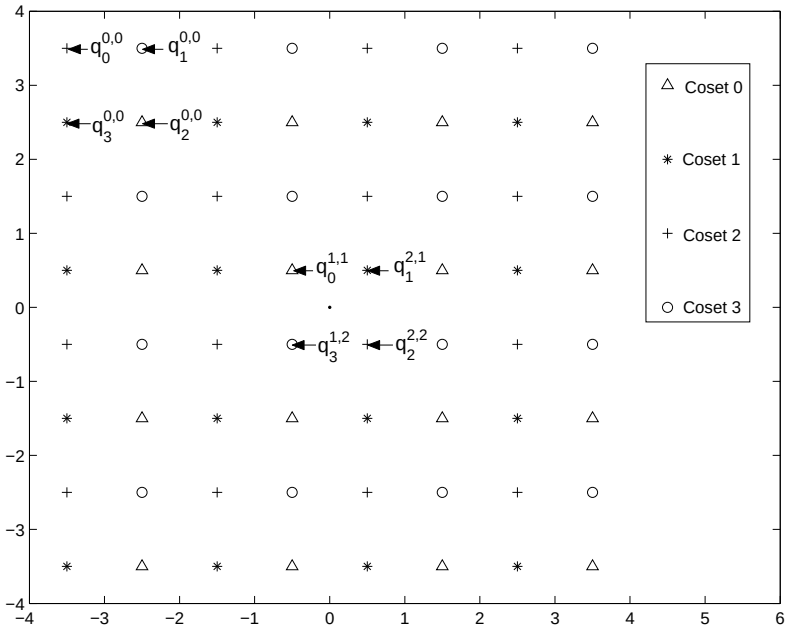

Fig. 15. Rate-$2\frac{1}{2}$ TCVQ codebook with 64 codewords.

dimension. The 2^{2R+2} code vectors are also partitioned into four cosets D_0, D_1, D_2, and D_3, each with 2^{2R+1} code vectors. A code vector is denoted as $q_c^{\mathbf{x},\mathbf{y}}$, where $c = 0, 1, 2, 3$ is the coset index, and $\mathbf{x}, \mathbf{y} : 0 \leq \mathbf{x}, \mathbf{y} \leq 2^{R+1} - 1$ are the indices of the code vector in x direction and y direction. Figure 15 is an example of such a 2-D uniform codebook for rate-$2\frac{1}{2}$ TCVQ with $2^{2*2+2} = 64$ code vectors. The quantization procedure of 2-D TCVQ is almost the same as that of TCQ except that

1. The trellises used in TCVQ are designed for $\mathbf{Z}_2$ signals, while those in TCQ are designed for $\mathbf{Z}_1$ signals.

2. The distortion is defined by the Euclidian distance between the code vector and the source vector.

3. The TCVQ index of each source vector $\vec{X}_i$ consists of one trellis bit and $2R$ "codeword bits". Hence the TCVQ rate is $2R + 1$ bits per two samples, i.e.,

$R + \frac{1}{2}$ b/s, among which only $\frac{1}{2}$ b/s is used to specify the trellis path.

To efficiently decode the TCVQ index sequence given the side information, we also need the conditional probability $P(Q(\vec{X}) = q_c^{\mathbf{x},\mathbf{y}}|\vec{X})$, i.e., $P(Q(\vec{X}) \in D_c|\vec{X})$. This time, if we partition the whole granular region into $N \times N$ mini-cells, the computation complexity will be intractable. Hence we only partition one Voronoi cell into $M \times M$ mini-cells (each of size $\delta \times \delta$ and is denoted as $\Delta_{x,y}$), and compute $P(Q(\vec{X}) = q_c^{\mathbf{x},\mathbf{y}}|\vec{X})$ for all $\vec{X}$ that belongs to that Voronoi cell. An example of partition with $M = 20$ is shown in Figure 16. For the source vectors outside this Voronoi cell, symmetric properties of the conditional probability $P(Q(\vec{X}) \in D_c|\vec{X})$ can be explored to map each of them into the basic Voronoi cell that is partitioned, because in the Viterbi algorithm, a source vector play its role via the distances from itself to the nearest code vectors in the four cosets. Hence it is the relative position instead of the absolute position of a source vector that really matters. For example, according to Figure 17, $\{P(Q(\vec{X}) \in D_c|\vec{X} = \vec{x}_i) : 1 \leq i \leq 9\}$ are equal for any $c = 0, 1, 2, 3$ because their relative positions to the four cosets are the same.

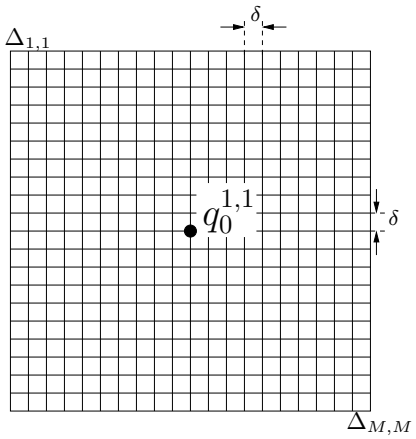

Fig. 16. Partition of a Voronoi cell with $M = 20$.

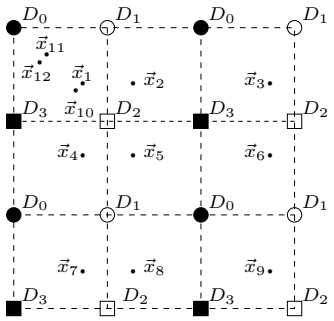

Fig. 17. Symmetric properties of $P(Q(\vec{X}) = q_c^{\mathbf{x},\mathbf{y}}|\vec{X})$.

Note that we can further reduce the complexity by a factor of four by assuming symmetry among the four cosets. For example,

$$\begin{aligned} & P(Q(\vec{X}) \in D_2|\vec{X} = \vec{x}_1) \quad = \quad P(Q(\vec{X}) \in D_2|\vec{X} = \vec{x}_{10}) \\ = \quad & P(Q(\vec{X}) \in D_0|\vec{X} = \vec{x}_{11}) \quad = \quad P(Q(\vec{X}) \in D_0|\vec{X} = \vec{x}_{12}); \end{aligned} \tag{3.15}$$

$$\begin{aligned} & P(Q(\vec{X}) \in D_1|\vec{X} = \vec{x}_1) \quad = \quad P(Q(\vec{X}) \in D_3|\vec{X} = \vec{x}_{10}) \\ = \quad & P(Q(\vec{X}) \in D_1|\vec{X} = \vec{x}_{11}) \quad = \quad P(Q(\vec{X}) \in D_3|\vec{X} = \vec{x}_{12}); \end{aligned} \tag{3.16}$$

$$\ldots \quad \ldots.$$

Hence, we only need $P(Q(\vec{X}) \in D_c|\vec{X})$ for $\vec{X}$ in one quarter of a Voronoi cell. Probabilities of any other point can be mapped into this quarter by symmetry. Figure 18 is an example of $P(Q(\vec{X}) \in D_c|\vec{X})$ for $\vec{X}$ in one Voronoi cell (we only compute $P(Q(\vec{X}) \in D_c|\vec{X})$ for a quarter of it, and extend them by symmetry) with $M = 40$. The shape is quite like that of a 2-D jointly Gaussian distribution.

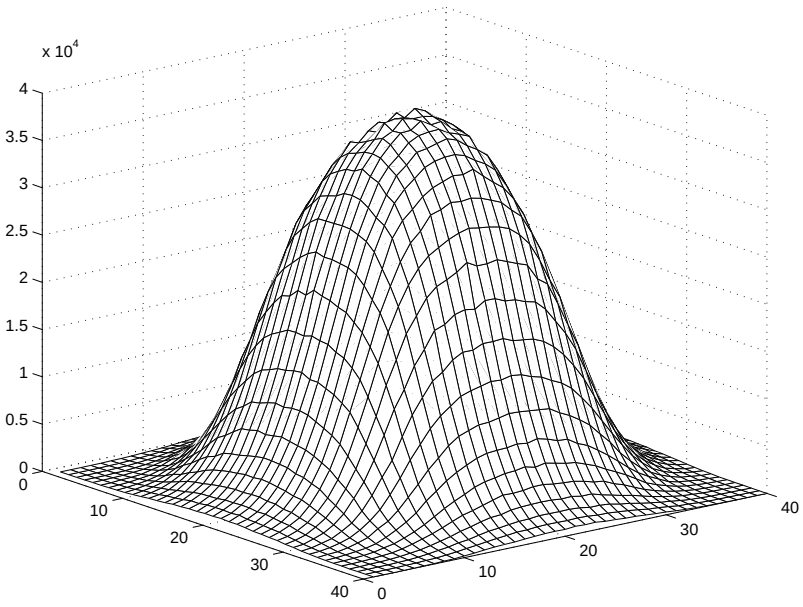

Fig. 18. $P(Q(\vec{X}) \in D_c|\vec{X})$ for $\vec{X}$ in one Voronoi cell.

D. Decoding Algorithms of the Codeword Bits

Based on the conditional probability $P(Q(X) = q_c^{\mathbf{b}}|X \in \Delta_n)$ for TCQ and $P(Q(\vec{X}) \in D_c|\vec{X} \in \Delta_{m,n})$ for TCVQ, we design algorithms for both decoding of codeword bits and estimation. Recall that the *Code Estimator* needs to output $LLR(b_i^r|b_i^0, \cdots, b_i^{r-1}, Y = y_i, C = c_i)$, which is related to $P(Q(X) = q_{c_i}^{\mathbf{b}_i}|Y = y_i)$. Unlike the 1-D and 2-D cases in [13], the main difficulty with SWC-TCQ is that $P(Q(X) = q_{c_i}^{\mathbf{b}_i}|Y = y_i)$ cannot be directly computed with integration. To solve this problem, we develop a novel method by means of *weighted summation*. In this thesis, we only provide the algorithms for TCQ based scheme, and those for TCVQ based scheme are just simple extensions to the vector case.

We note that the decoder has *a priori* information about TCQ from $P(Q(X) = q_c^{\mathbf{b}}|X \in \Delta_n)$ and the side information Y. In addition, when decoding the codeword

bits $\mathbf{b_i}$'s, the corresponding coset index c_i has already been decoded. Then, because $Y \to X \to Q(X)$ forms a Markov chain, for *each* c_i and all $\mathbf{b}^i$,

$$\begin{aligned}
& P(Q(X) = q_{c_i}^{\mathbf{b}_i} | Y = y_i) \\
= & \sum_{n=1}^{N} P(Q(X) = q_{c_i}^{\mathbf{b}_i}, x_i \in \Delta_n | Y = y_i) \\
= & \sum_{n=1}^{N} P(Q(X) = q_{c_i}^{\mathbf{b}_i} | x_i \in \Delta_n) P(x_i \in \Delta_n | Y = y_i) \\
= & \sum_{n=1}^{N} P(Q(X) = q_{c_i}^{\mathbf{b}_i} | x_i \in \Delta_n) \int_{\Delta_n} f_Z(x - y_i) dx \\
\approx & \ \delta \sum_{n=1}^{N} P(Q(X) = q_{c_i}^{\mathbf{b}_i} | x_i \in \Delta_n) f_Z(w_n - y_i). \qquad (3.17)
\end{aligned}$$

In 3.17 we have set x_i to w_n and the PDF $f_Z(x - y_i)$ to $f_Z(w_n - y_i)$ when $x_i \in \Delta_n$. This approximation is accurate only for large N. Our experiments show that the SNR gain of N=5000 over N=1000 is only 0.02 dB. Thus we set N=1000 throughout our simulations. $P(Q(X) = q_{c_i}^{\mathbf{b}_i} | x_i \in \Delta_n)$ in (1) comes from the look-up table $\{x_i, q_{c_i}^{\mathbf{b}_i}\}$. Another table for the exponential function in $f_Z(z)$ can also be employed to speed up the computation.

E. Optimal Estimation

Based on the same conditional probabilities, we first derive the conditional probabilities

$$\begin{aligned}
& P(x_i \in \Delta_n | Q(X) = q_{c_i}^{\mathbf{b}_i}, Y = y_i) \\
= & \ \frac{P(x_i \in \Delta_n, Q(X) = q_{c_i}^{\mathbf{b}_i} | Y = y_i)}{P(Q(X) = q_{c_i}^{\mathbf{b}_i} | Y = y_i)} \\
\overset{(a)}{=} & \ \frac{P(Q(X) = q_{c_i}^{\mathbf{b}_i} | x_i \in \Delta_n) P(x_i \in \Delta_n | Y = y_i)}{P(Q(X) = q_{c_i}^{\mathbf{b}_i} | Y = y_i)} \\
\overset{(b)}{\approx} & \ \frac{P(Q(X) = q_{c_i}^{\mathbf{b}_i} | x_i = w_n) f_Z(w_n - y_i)}{\sum_{n=1}^{N} P(Q(X) = q_{c_i}^{\mathbf{b}_i} | x_i = w_n) f_Z(w_n - y_i)}, \qquad (3.18)
\end{aligned}$$

where (a) is due to the Markov chain $Y \to X \to Q(X)$ and (b) is from (1). Then the optimal estimator is

$$\begin{aligned} & E(X|Q(X) = q_{c_i}^{\mathbf{b}_i}, Y = y_i) \\ = & \sum_{n=1}^{N} E(X|x_i \in \Delta_n, Q(X) = q_{c_i}^{\mathbf{b}_i}, Y = y_i) \\ & \cdot P(x_i \in \Delta_n | Q(X) = q_{c_i}^{\mathbf{b}_i}, Y = y_i) \\ = & \sum_{n=1}^{N} w_n P(x_i \in \Delta_n | Q(X) = q_{c_i}^{\mathbf{b}_i}, Y = y_i). \end{aligned} \tag{3.19}$$

This estimator is universal as it does not assume $Q(X) - X$ being Gaussian or independence of $Q(X) - X$ and Z. It outperforms the estimator in [11] that linearly combines $Q(X)$ and Y, especially at low rate.

F. Practical Slepian-Wolf Code Design Based on LDPC Codes

The goal of Slepian-Wolf coding is to achieve the conditional entropy $H(Q(X)|Y)$ after TCQ. By the chain rule,

$$H(Q(X)|Y) = H(\mathbf{b}^0|Y) + H(\mathbf{b}^1|\mathbf{b}^0, Y) + \cdots + H(\mathbf{b}^{R-1}|\mathbf{b}^0, \mathbf{b}^1, \cdots, \mathbf{b}^{R-2}, Y). \tag{3.20}$$

Practical designs are carried out to maximize the irregular LDPC code rates to compress $\mathbf{b}^0$ to $H(\mathbf{b}^0|Y)$ b/s and $\mathbf{b}^r$ to $H(\mathbf{b}^r|\mathbf{b}^1, \cdots, \mathbf{b}^{r-1}, Y)$ b/s for $1 \le r \le R-1$, respectively [14]. Decoding of $\mathbf{b}^0$ relies on $LLR(\mathbf{b}^0|Y)$ as described in Section 2. To decode b_i^r for $1 \le r \le R-1$, we compute

$$\begin{aligned} & LLR(b_i^r | \hat{b}_i^0, \cdots, \hat{b}_i^{r-1}, Y = y_i, C = c_i) \\ = & \log \frac{P(b_i^r = 0 | \hat{b}_i^0, \cdots, \hat{b}_i^{r-1}, Y = y_i, C = c_i)}{P(b_i^r = 1 | \hat{b}_i^0, \cdots, \hat{b}_i^{r-1}, Y = y_i, C = c_i)} \\ = & \log \frac{\sum_{b_i^r = 0 | \hat{b}_i^0, \cdots, \hat{b}_i^{r-1}} P(Q(X) = q_{c_i}^{\mathbf{b}_i} | Y = y_i)}{\sum_{b_i^r = 1 | \hat{b}_i^0, \cdots, \hat{b}_i^{r-1}} P(Q(X) = q_{c_i}^{\mathbf{b}_i} | Y = y_i)} \end{aligned} \tag{3.21}$$

based on (3.17) before running *LDPC Decoder II*. The multilevel LDPC codes based Slepian-Wolf decoding procedure is shown in Figure 19. More details are in [14].

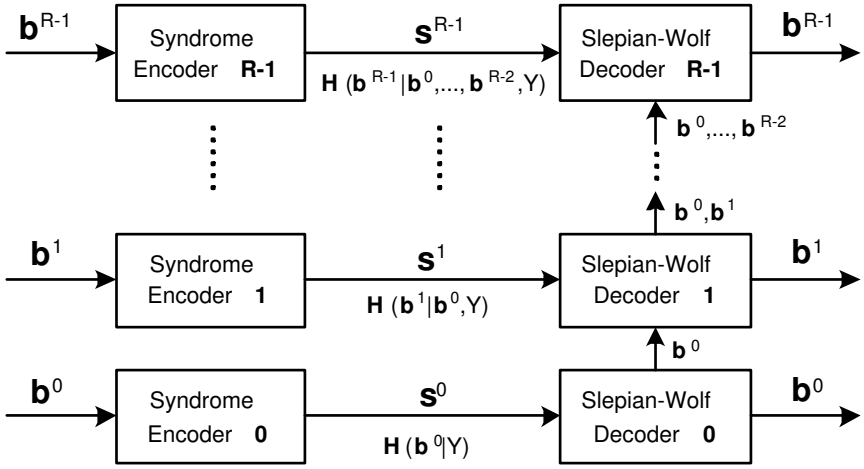

Fig. 19. Multilevel LDPC codes based Slepian-Wolf decoding procedure.

G. Results

Extensive simulations have been carried out to evaluate our proposed SWC-TCQ scheme. Assuming ideal Slepian-Wolf coding with rate computed from $H(Q(X)|Y)$, we find out that SWC-TCQ perform 0.2 dB away from $D^*_{WZ}(R)$ at high rate (e.g., 3 b/s), and that SWC-TCQ and SWC-TCVQ with optimal estimation (2) perform 0.67 dB and 0.38 dB, respectively, away from $D^*_{WZ}(R)$ at low rate (e.g., 1 b/s). These results and those in [13] reveal that the performance gap of high-rate Wyner-Ziv coding (with ideal Slepian-Wolf coding) to $D^*_{WZ}(R)$ is exactly the same as that of high-rate classic source coding (with ideal entropy coding) to the distortion-rate function $D_X(R)$. This interesting and important finding is highlighted in Table I. There is also a schematic connection between entropy-coded quantization for classic

source coding and Slepian-Wolf coded quantization (e.g., SWC-NQ [13] and SWC-TCQ) for Wyner-Ziv coding if one replaces a classic entropy coder by a syndrome based entropy coder using turbo or LDPC codes.

Table I. High-rate Wyner-Ziv coding vs. high-rate classic source coding in terms of the gap to the theoretical performance limit.

Classic source coding		Wyner-Ziv coding	
ECSQ	1.53 dB	SWC-NSQ	1.53 dB
ECLQ (2-D)	1.36 dB	SWC-NQ (2-D)	1.36 dB
ECTCQ	0.2 dB	SWC-TCQ	0.2 dB

With practical Slepian-Wolf coding based on irregular LDPC codes of length 10^6 bits, our SWC-TCQ coder performs 0.83 dB away from $D^*_{WZ}(R)$ at medium bit rates (e.g., ≥ 2.3 b/s) and 1.46 dB away from $D^*_{WZ}(R)$ at 1.1 b/s when $\sigma^2_Y = 1$ and $\sigma^2_Z = 0.28$. Our SWC-TCVQ coder performs 0.47 dB away from $D^*_{WZ}(R)$ at 3.3 b/s and 0.66 dB away from $D^*_{WZ}(R)$ at 1.0 b/s when $\sigma^2_Y = 1$ and $\sigma^2_Z = 0.10$. These results and more details are given in Figure 20 and Figure 21.

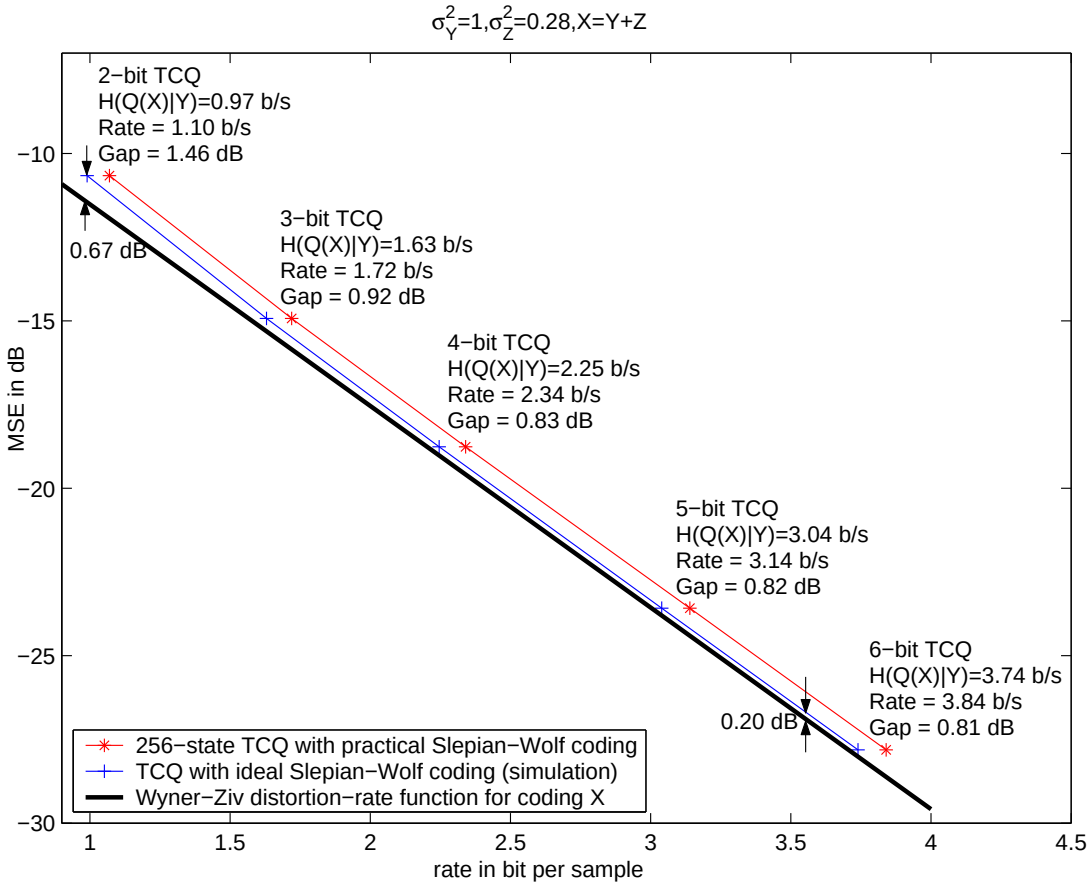

Fig. 20. Wyner-Ziv coding results based on TCQ and Slepian-Wolf coding. At high rate, ideal Slepian-Wolf coded TCQ performs 0.2 dB away from the theoretical limit. Results with practical Slepian-Wolf coding based on irregular LDPC codes are also included.

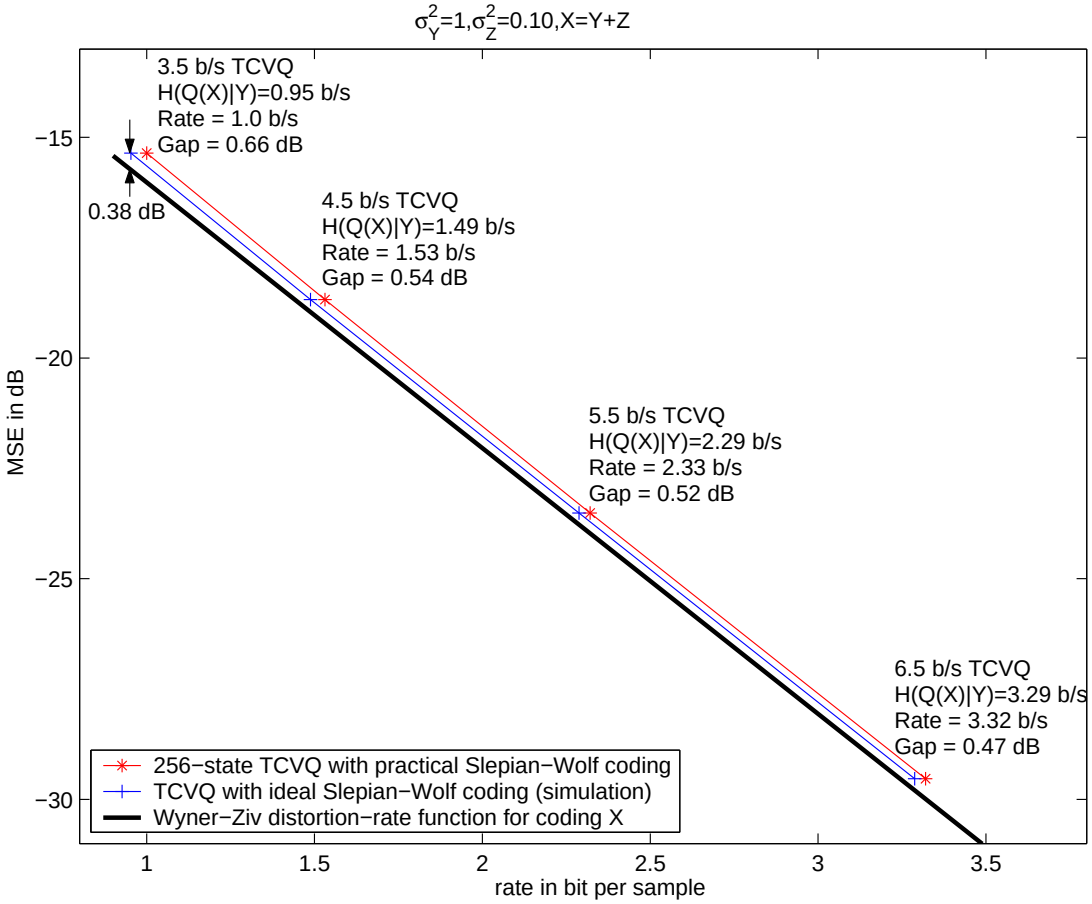

Fig. 21. Wyner-Ziv coding results based on TCVQ and Slepian-Wolf coding. At high rate, ideal Slepian-Wolf coded TCVQ performs 0.2 dB away from the theoretical limit.

CHAPTER IV

ASYMMETRIC MULTITERMINAL SOURCE CODE DESIGN

A. Gaussian Multiterminal Source Coding

The direct/indirect Gaussian multiterminal source coding system is depicted in Figure 22. Let X be a Gaussian random variable taking values in the real line $\mathcal{R}$ with

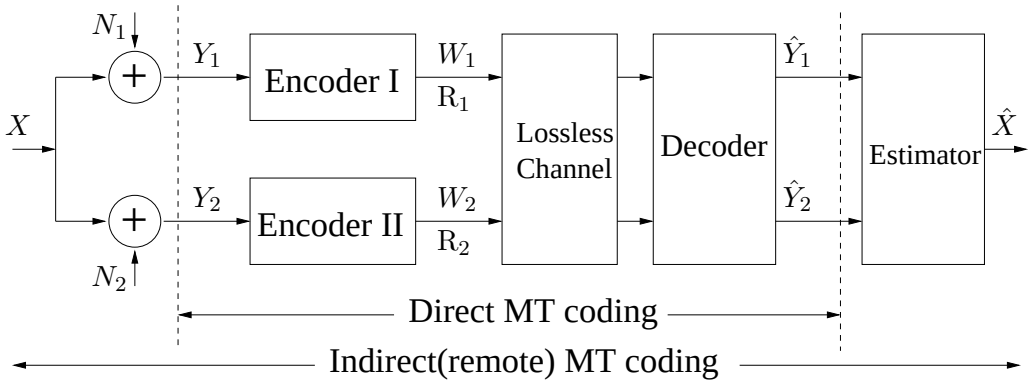

Fig. 22. Direct/indirect multiterminal source coding setup

variance σ_x^2. N_1 and N_2 are independent Gaussian random variables with the same variance σ_n^2. Y_1 and Y_2 are two noisy versions of X defined by $Y_1 = X + N_1$ and $Y_2 = X + N_2$. The covariance matrix Λ between Y_1 and Y_2 is

$$\Lambda = \begin{pmatrix} \sigma_x^2 + \sigma_n^2 & \sigma_x^2 \\ \sigma_x^2 & \sigma_x^2 + \sigma_n^2 \end{pmatrix} \tag{4.1}$$

The variances of Y_1 and Y_2 are $\sigma_{y_1}^2 = \sigma_{y_2}^2 = \sigma_y^2 = \sigma_x^2 + \sigma_n^2$, with the correlation coefficient $\rho = \sigma_x^2/(\sigma_x^2 + \sigma_n^2)$. In the indirect (remote) multiterminal problem, X represents the source which is symmetrically corrupted by noises N_1 and N_2, with Y_1 and Y_2 as separate observations. In the direct case, Y_1 and Y_2 themselves are

assumed to be jointly Gaussian sources defined by Λ. In both cases, Y_1 and Y_2 are separately encoded into W_1 and W_2 using rates R_1 and R_2, respectively. Let $Y_1^n = \{Y_{1,0}, Y_{1,1}, \ldots, Y_{1,n-1}\}$, $Y_2^n = \{Y_{2,0}, Y_{2,1}, \ldots, Y_{2,n-1}\}$ be n independent samples drawn from Y_1 and Y_2. The coded messages are denoted as $W_1 = \mathcal{E}_1(Y_1^n)$ and $W_2 = \mathcal{E}_2(Y_2^n)$ with the encoder functions $\mathcal{E}_1(\cdot)$ and $\mathcal{E}_2(\cdot)$ defined by

$$\begin{aligned} \mathcal{E}_1 &: \mathcal{R}^n \to \{1, 2, \ldots, 2^{nR_1}\} \\ \mathcal{E}_2 &: \mathcal{R}^n \to \{1, 2, \ldots, 2^{nR_2}\} \end{aligned} \tag{4.2}$$

Passed through noiseless channels, W_1 and W_2 are jointly decoded to form the reconstructions of both Y_1 and Y_2, denoted as $\hat{Y}_1 = \mathcal{D}_1(W_1, W_2)$ and $\hat{Y}_2 = \mathcal{D}_2(W_1, W_2)$. Hence, the decoder functions $\mathcal{D}_1(\cdot, \cdot)$ and $\mathcal{D}_2(\cdot, \cdot)$ are defined as

$$\begin{aligned} \mathcal{D}_1 &: \{1, 2, \ldots, 2^{nR_1}\} \times \{1, 2, \ldots, 2^{nR_2}\} \to \mathcal{R}^n \\ \mathcal{D}_2 &: \{1, 2, \ldots, 2^{nR_2}\} \times \{1, 2, \ldots, 2^{nR_2}\} \to \mathcal{R}^n \end{aligned} \tag{4.3}$$

Given $\hat{Y}_1$ and $\hat{Y}_2$, indirect multiterminal system needs another step to estimate the source $X^n = \{X_0, X_1, \ldots, X_{n-1}\}$ while direct multiterminal system does not. The estimator function $\mathcal{S}(\cdot, \cdot)$, which reconstructs X^n to $\hat{X}^n = \mathcal{S}(Y_1, Y_2)$, is a mapping

$$\mathcal{S} : \mathcal{R}^n \times \mathcal{R}^n \to \mathcal{R}^n \tag{4.4}$$

Written in a single formula, the encoding, decoding, and estimation functions for direct/indirect multiterminal coding system can be combined as

$$\begin{aligned} \textit{direct}: &\qquad \hat{Y}_i = \mathcal{D}_i(\mathcal{E}_1(Y_1), \mathcal{E}_2(Y_2)) \quad \textit{for} \;\; i = 1, 2 \\ \textit{indirect}: &\quad \hat{X} = \mathcal{S}(\mathcal{D}_1(\mathcal{E}_1(Y_1), \mathcal{E}_2(Y_2)), \mathcal{D}_2(\mathcal{E}_1(Y_1), \mathcal{E}_2(Y_2))) = \mathcal{D}(\mathcal{E}_1(Y_1), \mathcal{E}_2(Y_2)) \end{aligned} \tag{4.5}$$

where $\mathcal{D}(\cdot, \cdot)$ is the concatenated decoder function for remote case.

Let the distortion measure be the MSE, i.e.,

$$d(X^n, Y^n) = \frac{1}{n}\sum_{i=0}^{n-1}(X_i - Y_i)^2. \tag{4.6}$$

For a target distortion D, the achievable rate region of indirect multiterminal problem is the set of all the rate pairs (R_1, R_2) for which there exist functions $\mathcal{E}_1(\cdot)$, $\mathcal{E}_2(\cdot)$, and $\mathcal{D}(\cdot,\cdot)$ such that

$$E[d(X, \hat{X})] \leq D. \tag{4.7}$$

Similarly, the achievable rate region of direct multiterminal problem is defined for given distortion pairs (D_1, D_2), with two distortion constraints

$$E[d(Y_1, \hat{Y}_1)] \leq D_1, \quad E[d(Y_2, \hat{Y}_2)] \leq D_2. \tag{4.8}$$

B. Achievable Rate Region

The inner bound for the direct multiterminal setting is given in [17, 21] as

$$R_1 \geq I(Y_1; Z_1) - I(Z_1; Z_2), \tag{4.9}$$

$$R_2 \geq I(Y_2; Z_2) - I(Z_1; Z_2), \tag{4.10}$$

$$R_1 + R_2 \geq I(Y_1Y_2; Z_1Z_2), \tag{4.11}$$

where Z_1 and Z_2 are auxiliary random variables satisfying a Markov chain $Z_1 \rightarrow Y_1 \rightarrow Y_2 \rightarrow Z_2$, and there exist functions $\hat{Y}_1 = g_1(Z_1, Z_2)$ and $\hat{Y}_2 = g_2(Z_1, Z_2)$ such that distortion constraints (4.8) are satisfied. The inner bound for the indirect case [22, 23] is also given by (4.9) – (4.11) where Z_1 and Z_2 are such that $Z_1 \rightarrow Y_1 \rightarrow X \rightarrow Y_2 \rightarrow Z_2$ holds, and there exists a function $\hat{X} = g(Z_1, Z_2)$ satisfying distortion constraint (4.7).

1. Quadratic Gaussian Indirect Multiterminal Problem

Using test channels $\hat{Y}_i = Y_i + Q_i$, $i = 1, 2$, where Q_i is an i.i.d. variable independent of Y_i and $Q_i \sim \mathcal{N}(0, \sigma_{q_i}^2)$, Yamamoto and Itoh [22] report the following achievable rate region:

$$R_1 \geq \frac{1}{2} \log \frac{\sigma_x^2(\sigma_n^2 + \sigma_{q_1}^2) + \sigma_x^2(\sigma_n^2 + \sigma_{q_2}^2) + (\sigma_n^2 + \sigma_{q_1}^2)(\sigma_n^2 + \sigma_{q_2}^2)}{\sigma_{q_1}^2(\sigma_x^2 + \sigma_n^2 + \sigma_{q_2}^2)}, \tag{4.12}$$

$$R_2 \geq \frac{1}{2} \log \frac{\sigma_x^2(\sigma_n^2 + \sigma_{q_2}^2) + \sigma_x^2(\sigma_n^2 + \sigma_{q_1}^2) + (\sigma_n^2 + \sigma_{q_2}^2)(\sigma_n^2 + \sigma_{q_1}^2)}{\sigma_{q_2}^2(\sigma_x^2 + \sigma_n^2 + \sigma_{q_1}^2)}, \tag{4.13}$$

$$R = R_1 + R_2 \geq \frac{1}{2} \log \frac{\sigma_x^2(\sigma_n^2 + \sigma_{q_1}^2) + \sigma_x^2(\sigma_n^2 + \sigma_{q_2}^2) + (\sigma_n^2 + \sigma_{q_1}^2)(\sigma_n^2 + \sigma_{q_2}^2)}{\sigma_{q_1}^2 \sigma_{q_2}^2}, \tag{4.14}$$

where $\sigma_{q_1}^2$ and $\sigma_{q_2}^2$ are selected so that

$$d = \frac{1}{\frac{1}{\sigma_x^2} + \frac{1}{\sigma_n^2 + \sigma_{q_1}^2} + \frac{1}{\sigma_n^2 + \sigma_{q_2}^2}}. \tag{4.15}$$

The optimal estimation function is given by $g(\hat{Y}_1, \hat{Y}_2) = \gamma_1 \hat{Y}_1 + \gamma_2 \hat{Y}_2$. Recently, it is proved that this bound is tight [25].

In practice, it is usually desirable to minimize the sum rate $R = R_1 + R_2$. The following lemma shows how to do it efficiently.

Lemma 1 The sum rate $R = R_1 + R_2$ is minimum iff $\sigma_{q_1}^2 = \sigma_{q_2}^2$. The lemma is stated in [26, 24]. For completeness, we give here the rigorous proof.

Proof: We prove the lemma by contradiction. Suppose that there exist $\sigma_{q_1}^{*2}$ and $\sigma_{q_2}^{*2}$, such that $\sigma_{q_1}^{*2} \neq \sigma_{q_2}^{*2}$ and the sum rate (4.14) is minimum. Then, for any $\sigma_{q_1}^2 = \sigma_{q_2}^2 = \sigma_q^2$ that satisfies (4.15) we have

$$\frac{1}{2} \log \frac{(a + b_1^*) + (a + b_2^*) + (a + b_1^*)(a + b_2^*)}{b_1^* b_2^*} \leq \frac{1}{2} \log \frac{2(a + b) + (a + b)^2}{b^2}, \tag{4.16}$$

where we set $a = \sigma_n^2/\sigma_x^2$, $b_i^* = \sigma_{q_i}^{*2}/\sigma_x^2$, $i = 1, 2$, and $b = \sigma_q^2/\sigma_x^2$.

Let further $T_1 = a + b_1^*$, $T_2 = a + b_2^*$, and $T = a + b$. Then, (4.16) can be written in an equivalent form:

$$\frac{T + T + T^2}{b^2} \geq \frac{T_1 + T_2 + T_1 T_2}{b_1^* b_2^*}, \tag{4.17}$$

or

$$b_1^* b_2^* T^2 \frac{T + T + T^2}{T^2} \geq b^2 T_1 T_2 \frac{T_1 + T_2 + T_1 T_2}{T_1 T_2}. \tag{4.18}$$

On the other hand, since in both cases the distortion criterion must hold, we have

$$\frac{T + T + T^2}{T^2} = \frac{T_1 + T_2 + T_1 T_2}{T_1 T_2}. \tag{4.19}$$

Using this, we can simplify (4.18) to

$$b_1^* b_2^* T^2 \geq b^2 T_1 T_2. \tag{4.20}$$

From $T = a + b$ and (4.19), b can be expressed as:

$$b = \frac{2T_1 T_2 - aT_1 - aT_2}{T_1 T_2}. \tag{4.21}$$

By combining (4.20) and (4.21) we get

$$b_1^* b_2^* T_1 T_2 \geq (2T_1 T_2 - aT_1 - aT_2)^2, \tag{4.22}$$

or after replacing T_1 and T_2 by $a + b_1^*$ and $a + b_2^*$, respectively,

$$4b_1^* b_2^* (a^2 + ab_1^* + ab_2^* + b_1^* b_2^*) \geq (ab_1^* + ab_2^* + 2b_1^* b_2^*)^2. \tag{4.23}$$

From here, after simple calculations we obtain $(b_1^* - b_2^*)^2 \leq 0$. Since our assumption is $b_1^* \neq b_2^*$, the last expression cannot be satisfied. Thus, we came to a contradiction.

For $\sigma_{q_1}^2 = \sigma_{q_2}^2 = \sigma_q^2$ the achievable bounds become:

$$R_i \geq \frac{1}{2} \log^+ [\frac{2\sigma_x^2}{\sigma_x^2 + D} \cdot (1 - \frac{\sigma_n^2(\sigma_x^2 - D)}{2\sigma_x^2 D})^{-1}], i = 1, 2 \tag{4.24}$$

$$R_1 + R_2 \geq \frac{1}{2}\log^+[\frac{\sigma_x^2}{D} \cdot (1 - \frac{\sigma_n^2(\sigma_x^2 - D)}{2\sigma_x^2 D})^{-2}], \tag{4.25}$$

where (X, N_1, N_2) are jointly Gaussian with variances $(\sigma_x^2, \sigma_n^2, \sigma_n^2)$ and

$$\log^+ x = \max\{\log x, 0\}. \tag{4.26}$$

In Figure 23 we present the achievable rate region given by inequalities (4.24) and (4.12) (which is proved to be tight [25]) together with the sum rate bound (4.24) – (4.25).

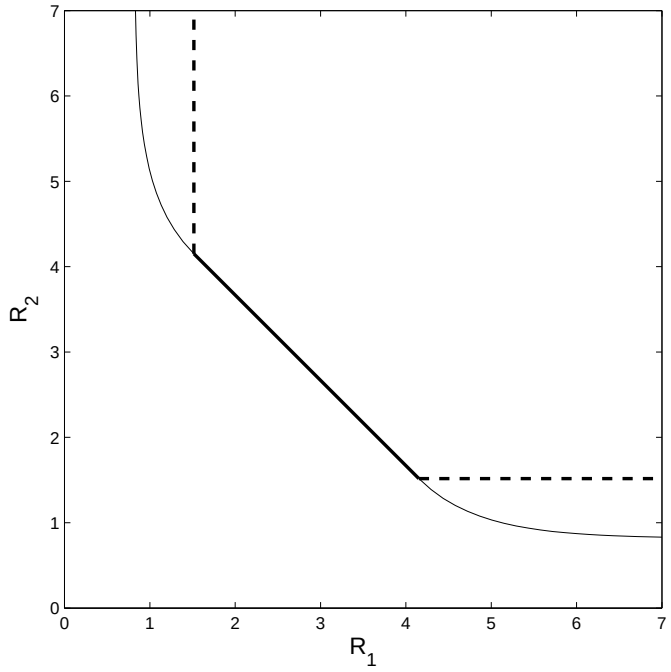

Fig. 23. The achievable rate region (solid lines, tight) and the sum rate bound (dashed lines) for indirect multiterminal source coding.

For a given fidelity criterion, the corner points $A = (R_1^*, R_2^*)$ and $B = (R_2^*, R_1^*)$ are given by

$$R_1^* = \frac{1}{2}\log^+[\frac{\sigma_x^2 + D}{2D} \cdot (1 - \frac{\sigma_n^2(\sigma_x^2 - D)}{2\sigma_x^2 D})^{-1}], \tag{4.27}$$

and

$$R_2^* = \frac{1}{2}\log^+[\frac{2\sigma_x^2}{\sigma_x^2 + D} \cdot (1 - \frac{\sigma_n^2(\sigma_x^2 - D)}{2\sigma_x^2 D})^{-1}]. \tag{4.28}$$

It is interesting to see whether there exists a distortion d such that the sum rate is minimum only for one rate pair (R_1, R_2); in this case, the line between A and B reduces to a single point. The following lemma gives the answer to this question.

Lemma 2 Let $\mathcal{R}$ be the set of all achievable (R_1, R_2) pairs. Then, the solution of the minimization problem $\min_{(R_1,R_2)\in\mathcal{R}} R_1 + R_2$ is unique iff $d \geq \sigma_x^2$, and it is given by $R_1 = R_2 = 0$.

Proof: It is shown in [24] that the sum rate $R = R_1 + R_2$ is minimum when $R_1 = R_2$. Thus, it is enough to find the condition when the points A and B overlap. Then, the result of the lemma immediately follows from (4.24) and (4.25) by setting $R_1 + R_2 = 2R_1$.

Thus, we have a unique solution to the minimization problem only in the trivial case when nothing is transmitted. Whenever $d < \sigma_x^2$, the bound has a line portion. Recall that the achievability of the bound is proved using the test channels $\hat{Y}_i = Y_i + Q_i$, $i = 1, 2$, where Q_i is Gaussian and independent of Y_i. Required independence of the quantization error Q_i suggests the use of a dithering signal. On the other hand, infinite-dimension lattice codes produce Gaussian output. Thus, as shown by Zamir, Shamai, and Erez [29], by exploiting entropy-coded dithered quantization (ECDQ) with infinite-dimension nested lattice codes, the theoretical limit can be reached. We attempt to approximately satisfy both requirements by using TCQ with a uniformly distributed dither. However, since TCQ does not provide strictly Gaussian noise, certain performance loss is expected.

2. Quadratic Gaussian Direct Multiterminal Problem

For the direct Gaussian multiterminal problem, where (Y_1, Y_2) are jointly Gaussian with variances $(\sigma^2_{y1}, \sigma^2_{y2})$ and correlation coefficient $\rho = \frac{E[Y_1 Y_2]}{\sigma_{y1}\sigma_{y2}}$, the inner bound is [18]

$$R_1 \geq \frac{1}{2}\log[\frac{\sigma^2_{y_1}}{D_1}(1-\rho^2+\rho^2 2^{-2R_2})], \tag{4.29}$$

$$R_2 \geq \frac{1}{2}\log[\frac{\sigma^2_{y_2}}{D_2}(1-\rho^2+\rho^2 2^{-2R_1})], \tag{4.30}$$

$$R_1 + R_2 \geq \frac{1}{2}\log[(1-\rho^2)\frac{\beta_{max}\sigma^2_{y_1}\sigma^2_{y_2}}{2D_1D_2}], \tag{4.31}$$

where

$$\beta_{max} = 1 + \sqrt{1 + \frac{4\rho^2 D_1 D_2}{(1-\rho^2)^2\sigma^2_{y_1}\sigma^2_{y_2}}}, \tag{4.32}$$

And the outer bound [17, 21] is defined by (4.29), (4.30) and

$$R_1 + R_2 \geq \frac{1}{2}\log[(1-\rho^2)\frac{\sigma^2_{y_1}\sigma^2_{y_2}}{D_1D_2}]. \tag{4.33}$$

We see that even in this special case, the inner bound and the outer bound do not coincide. There is still an uncertainty region where achievability is unknown, the width of the uncertainty region is $\frac{1}{2}\log[\frac{\beta_{max}}{2}]$. Figure 24 shows an example of the inner and outer bounds for direct multiterminal setting.

C. Code Design for the Indirect Mmultiterminal Setting

We consider the quadratic Gaussian case, where the source $X \sim \mathcal{N}(0, \sigma_x^2)$ is observed by two encoders. The encoders' observations are given by: $Y_i = X + N_i$, $i = 1, 2$, where $N_i \sim \mathcal{N}(0, \sigma_n^2)$ is independent of X. At the first encoder, Y_1 is quantized by TCQ1 and sent. The second encoder first quantizes Y_2 by TCQ2, and then by exploiting the remaining correlation between quantized observations, it attempts to reduce the

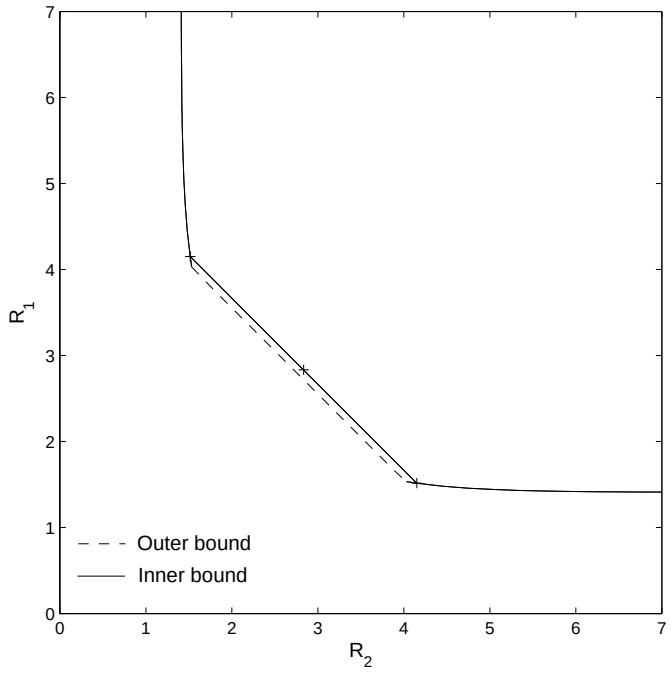

Fig. 24. The inner (solid lines) and outer bounds (dashed lines) for direct multiterminal source coding.

sending rate to $H(\hat{Y}_1|\hat{Y}_2)$, where $\hat{Y}_1$ and $\hat{Y}_2$ are reconstructions of the observations after TCQ decoding. Before the quantization, a dither uniformly distributed over a Voronoi region corresponding to the uniform-threshold scalar quantizer is added to make the quantization noise $Q(Y_i)$, $i = 1, 2$, independent of the input signal [29].

We explain in more details coding of Y_2, which is depicted in Figure 25. Coding is done in blocks of length N samples each. The samples are first independently quantized with an R-bit TCQ quantizer. The obtained index sequence is given by $\mathbf{B} = \{\mathbf{b}^0, \mathbf{b}\}$, where $\mathbf{b}^0$ is a trellis bit sequence and $\mathbf{b} = \{\mathbf{b}^1, \mathbf{b}^2, \cdots, \mathbf{b}^{R-1}\}$ denotes codeword bit sequences. For $i = 1, \ldots, N$, let $\mathbf{B}_i = \{b_i^0, \mathbf{b}_i\} = \{b_i^0, b_i^1, \cdots, b_i^{R-1}\}$ be the i-th such index.

The *Syndrome Encoder* compresses $\mathbf{B}$ bit-plain by bit-plain into R syndrome

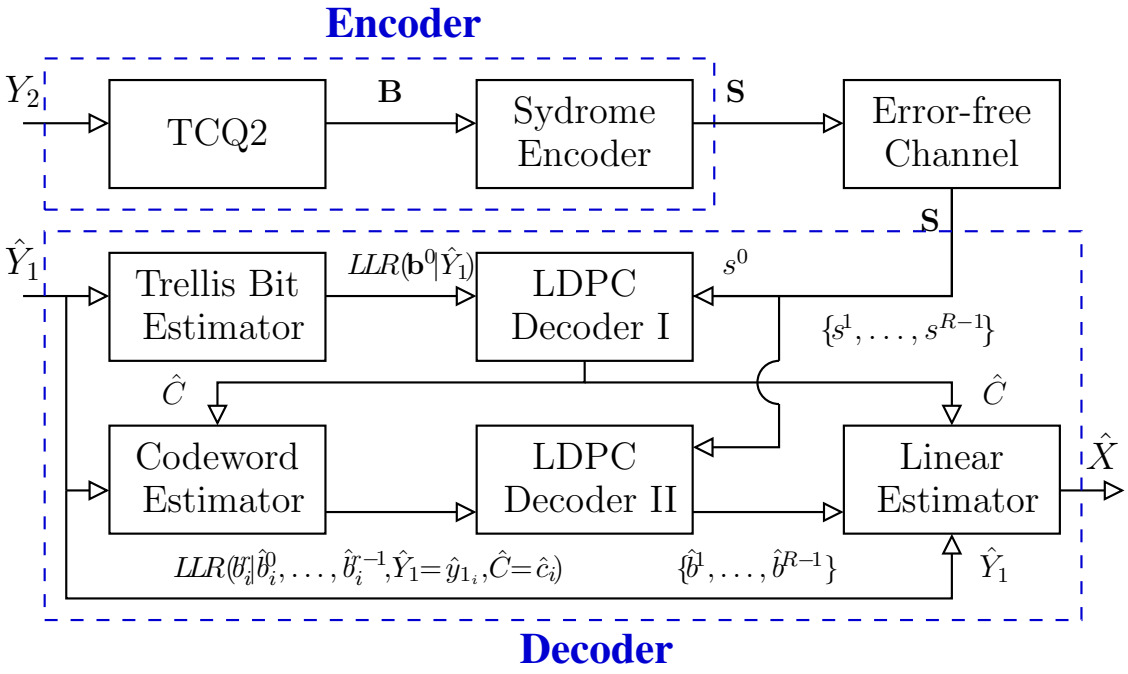

Fig. 25. Block diagram of TCQ-LDPC scheme for coding Y_2.

sequences $\mathbf{S} = \{\mathbf{s}^0, \mathbf{s}^1, \cdots, \mathbf{s}^{R-1}\}$ using R LDPC code of different rates [14].

At the receiver, $\hat{Y}_1$ plays the role of side information. To get the use of the side information, we must estimate remained correlation between Y_2 and $\hat{Y}_1$. Under the assumption that $(Y_1 Y_2 \hat{Y}_1 \hat{Y}_2)$ are jointly Gaussian, we express Y_2 as $Y_2 = \alpha \hat{Y}_1 + Z$, where $\alpha = \frac{\sigma_x^2 - d}{\sigma_x^2 + d}$ and $Z \sim \mathcal{N}(0, \sigma_z^2)$ is an i.i.d. random variable with variance $\sigma_z^2 = \frac{2\sigma_x^2 d}{\sigma_x^2 + d}$ and is independent of $\hat{Y}_1$.

For SW decoding, the log-likelihood ratios (LLRs) of the trellis bits $\mathbf{b}^0$ and codeword $\mathbf{b_i}$ sequences given side information are needed [14]. To obtain this information, we generate independent noise $Z \sim \mathcal{N}(0, \sigma_z^2)$, whose distribution is assumed to be known at the decoder, and simulate TCQ2 of $\alpha \hat{Y}_1 + Z$. *LDPC Decoder I* then reconstructs $\hat{\mathbf{b}}^0$ from the syndrome sequence $\mathbf{s}^0$ and $LLR(\mathbf{b}^0|\hat{Y}_1)$ [14]. $\hat{\mathbf{b}}^0$ determines the reconstructed coset index sequence $\hat{C}$. Using $\hat{C}$ and $\hat{Y}_1$ the *Codeword Estimator*

computes $LLR(b_i^r|\hat{b}_i^0,\cdots,\hat{b}_i^{r-1},\hat{Y}_1=\hat{y}_{1_i},\hat{C}=\hat{c}_i)$ for $1\leq r\leq R-1$. This is done on sample base by extracting key information from the trellis bits and combining it with the available side information. Indeed, let the quantized version of the i-th input sample be $q_{\hat{c}_i}^{\mathbf{b}_i}$, where $\hat{c}_i\in\{0,1,2,3\}$ is the coset index (we assume here a four coset quantizer). Then, using the similar technique as in [32] for i-th source sample we get

$$\begin{aligned}
& P(\hat{Y}_2=q_{\hat{c}_i}^{\mathbf{b}_i}|\hat{Y}_1=\hat{y}_{1_i}) \\
= & \sum_{k=1}^{n} P(\hat{Y}_2=q_{\hat{c}_i}^{\mathbf{b}_i},y_{2_i}\in\Delta_k|\hat{Y}_1=\hat{y}_{1_i}) \\
= & \sum_{k=1}^{n} P(\hat{Y}_2=q_{\hat{c}_i}^{\mathbf{b}_i}|y_{2_i}\in\Delta_k)P(Y_i\in\Delta_k|\hat{Y}_1=\hat{y}_{1_i}) \\
= & \sum_{k=1}^{n} P(\hat{Y}_2=q_{\hat{c}_i}^{\mathbf{b}_i}|y_{2_i}\in\Delta_k)\int_{\Delta_k} f_Z(x-\hat{y}_{1_i})dx \\
\approx & \ \delta\sum_{k=1}^{n} P(\hat{Y}_2=q_{\hat{c}_i}^{\mathbf{b}_i}|y_{2_i}\in\Delta_k)f_Z(w_k-\hat{y}_{1_i}),
\end{aligned} \tag{4.34}$$

where we discretized the system by uniformly partitioning the granular region of our uniform-threshold quanitizer into n length-δ mini-cells, $\Delta_1,\Delta_2,\ldots,\Delta_n$, and denote w_k as the mid-point of Δ_k for $1\leq k\leq n$. Note that, because $\mathbf{b}_i$ is unique given $\hat{c}_i$ for any y_{2_i}, the domain of $\hat{Y}_2$ given that $\hat{C}=\hat{c}_i$ is the whole real number line $\mathcal{R}$ for each $\hat{c}_i$. In (4.34) for $y_{2_i}\in\Delta_k$, we set $y_{2_i}=w_k$ and the PDF of the noise Z to $f_Z(w_k-\hat{y}_{1_i})$. Now, LLRs are computed as:

$$\begin{aligned}
& LLR(b_i^r|\hat{b}_i^0,\cdots,\hat{b}_i^{r-1},\hat{Y}_1=\hat{y}_{1_i},\hat{C}=\hat{c}_i) \\
= & \log\frac{P(b_i^r=0|\hat{b}_i^0,\cdots,\hat{b}_i^{r-1},\hat{Y}_1=\hat{y}_{1_i},\hat{C}=\hat{c}_i)}{P(b_i^r=1|\hat{b}_i^0,\cdots,\hat{b}_i^{r-1},\hat{Y}_1=\hat{y}_{1_i},\hat{C}=\hat{c}_i)} \\
= & \log\frac{\sum_{b_i^r=0|\hat{b}_i^0,\cdots,\hat{b}_i^{r-1}}P(\hat{Y}_2=q_{\hat{c}_i}^{\mathbf{b}_i}|\hat{Y}_1=\hat{y}_{1_i})}{\sum_{b_i^r=1|\hat{b}_i^0,\cdots,\hat{b}_i^{r-1}}P(\hat{Y}_2=q_{\hat{c}_i}^{\mathbf{b}_i}|\hat{Y}_1=\hat{y}_{1_i})}.
\end{aligned} \tag{4.35}$$

Using this, *LDPC Decoder II* reconstructs codeword sequences $\hat{\mathbf{b}}$. Then, $\hat{Y}_2$ is recovered by combining output of LDPC decoder and reconstructed coset index $\hat{C}$. Finally, we estimate the source using optimal linear estimator: $\hat{X}=\gamma\hat{Y}_1+\gamma\hat{Y}_2$, where

$\gamma = \frac{1}{2}(1 - \frac{d}{\sigma_x^2})$.

By varying the rate allocation between the two encoders, the proposed scheme can potentially reach all points on the dash lines in Figure 26. However, the rate allocation point on the dash line which minimizes the sum rate corresponds exactly to one of the corner points (A and B) of the achievable rate region which follows directly from the achievability of the sum rate bound [22]. Thus, in the next section, by minimizing the sum rate in our scheme we are able to approach points A and B.

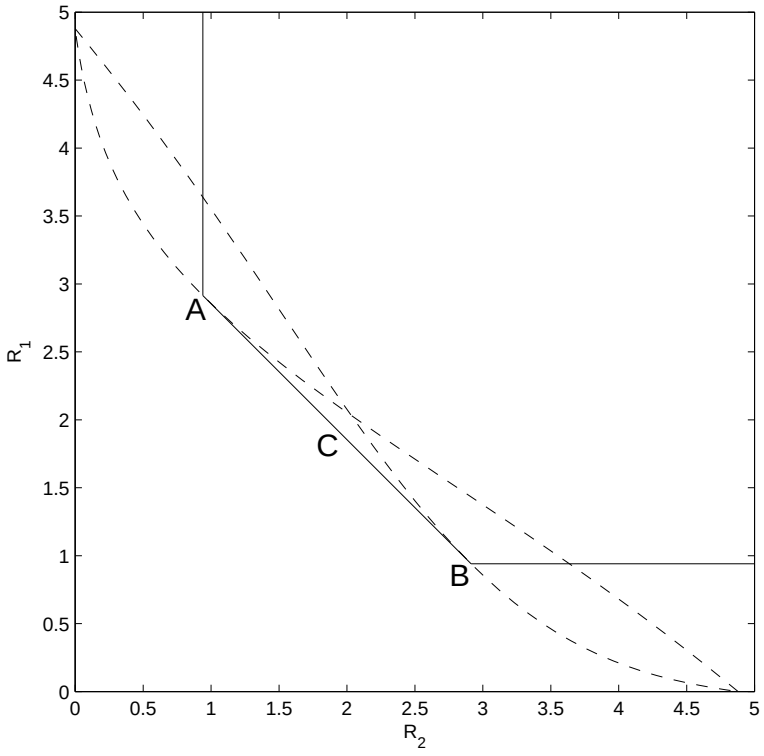

Fig. 26. The achievable rate allocations of our system (dashed lines) together with the inner sum rate bound (solid lines).

D. Results

In this section, we give our experimental results obtained with the scheme described in Section 3. However, to achieve non-integer rates, we replaced TCQ2 by trellis coded vector quantizer (TCVQ). In all our simulations, we assume that the source signal X is i.i.d. Gaussian with zero mean and $\sigma_x^2 = 1$. Noisy observations are given by: $Y_1 = X + N_1$ and $Y_2 = X + N_2$, where N_1 and N_2 are i.i.d. zero mean Gaussian with variance σ_n^2 and are independent of each other and X. We refer to the ratio σ_x^2/σ_n^2 as *correlation signal to noise ratio* (CSNR).

First we attempt to approach the corner points (A and B) on the achievable rate region by using Lemma 1; that is, $\sigma_q^2 = \sigma_{q_1}^2 = \sigma_{q_2}^2$. Then, for a fixed distortion d and CSNR, by varying the step size of TCQ1, we obtained quantization noise given by (4.15). The same quantization step size was used at the second encoder. Then, we performed Wyner-Ziv coding of the second observation using the quantization of the first as side information, as explained in the previous section. Obtained results together with the achievable bound are presented in Figure 27. Average distortion is $d = -17.75$ dB and CSNR=18 dB. *Ideal* results refer to ideal Slepian-Wolf coding. For practical results, we used irregular LDPC codes of length 10^6; error-free transmission was assumed if probability of error was less than 10^{-6}. The first observation Y_1 was only quantized and transmitted. The loss to R_1^* given by (4.27) was 0.03 bits per sample (b/s), which matches the loss of TCQ to rate-distortion function. The gap in Wyner-Ziv coding of Y_2 to R_2^* (4.28) assuming ideal Slepian-Wolf coding was 0.07 b/s. With the perfect Gaussian side information, the obtained loss was 0.063 b/s [32]. Thus, a very small performance loss is observed due to the imposed Gaussian approximation of the quantization noise. We had additional loss of 0.05 b/s due to practical LDPC based Slepian-Wolf coding; this is comparable with the results

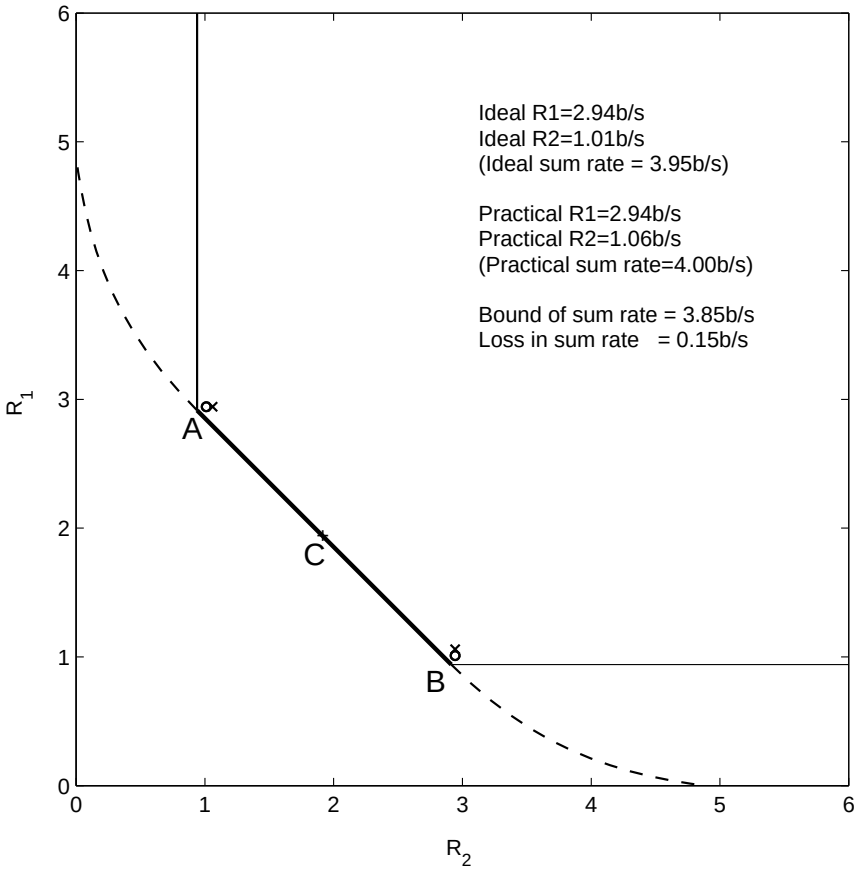

Fig. 27. Obtained experimental results together with the achievable rate region for CSNR=18 dB and $d = -17.75$ dB.

reported in [14], which justifies introduced Gaussian assumptions in the computation of LLRs.

We next compare our scheme to that of [36, 26] for different CSNRs and the sum rate equal to 4 b/s. We show results of the best scheme of [36, 26] which exploits 8-level Lloyd-Max fixed-length scalar quanitizer and 32-state trellis codes; it is employed in both the asymmetric and symmetric (the rates of both encodes are equal) setup. Obtained average distortion performance as a function of CSNR for our and the scheme of [36, 26] together with the achievable bound is presented in

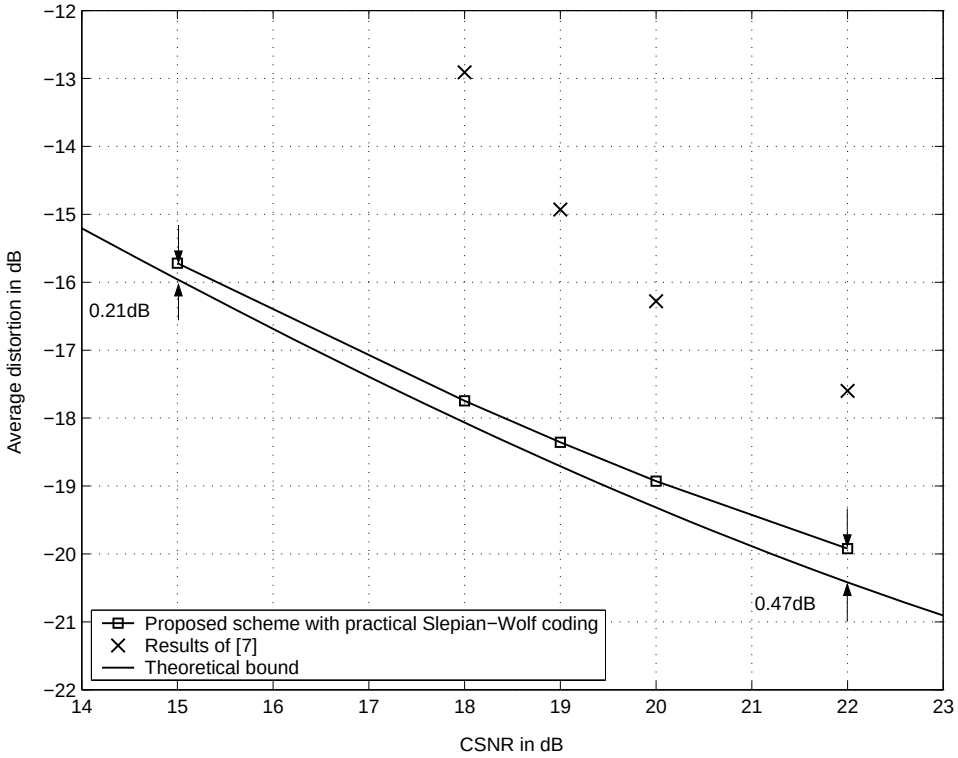

Fig. 28. Average distortion in dB as a function of CSNR for our TCQ-LDPC scheme, the best scheme of [26], together with the theoretical bound. The sum rate is 4 b/s.

Figure 28. It can be seen that our scheme significantly outperforms that in [36, 26]. Moreover, for the used range of CSNR the loss to the theoretical bound was at most 0.5 dB. As it can be seen, the gap of our scheme to the bound slightly increases with the CSNR increase. However, the loss in the sum rate was always around 0.15 b/s, and the constant rate loss produces increasing gap to the distortion bound.

CHAPTER V

MULTITERMINAL SOURCE CODE DESIGN BASED ON SOURCE SPLITTING

Although the asymmetric coding approach in chapter IV shows much better results than those of [26], it is limited to approaching only the two corner points on the achievable limit. In this chapter, based on the idea of [29], we provide a code design based on source splitting for direct and indirect multiterminal coding problems which contains a classical source coding component and two Wyner-Ziv coding components. Entropy-coded TCQ [31] with dithered uniform codebook is employed for classical source coding, and SWC-TCQ [32] is used in each of the two Wyner-Ziv coding components. Assuming ideal source coding and ideal Wyner-Ziv coding, we prove that this design is capable of achieving any rate point on the theoretical bounds for both the direct and indirect multiterminal problems in the quadratic Gaussian setting. Practical designs based on entropy-coded TCQ for source coding and SW-coded TCQ for Wyner-Ziv coding significantly outperform those of [26] and come very close to the theoretical limits in both multiterminal problems.

The organization is as follows. In section A, we introduce the proposed code design for both the direct and indirect multiterminal problems, Theoretical analysis and rigorous proofs of achievabilities of any point on the inner bounds are given in section B. After practical code design and results shown and discussed in section C, we conclude this chapter in the last section.

A. Proposed Code Design

In this section, we describe our code design (Figure 29) based on source splitting for direct and indirect multiterminal source coding with two encoders. The sources, e.g., X, are grouped into blocks of length n, e.g., $X^n = \{X_1, X_2, \ldots, X_n\}$, where X_i is the

i-th sample in the block.

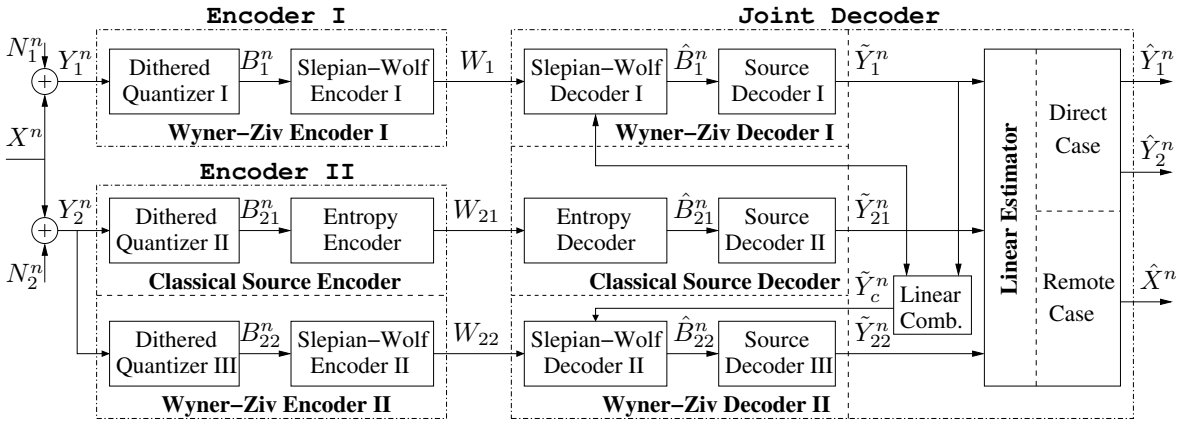

Fig. 29. Block diagram of the proposed multiterminal source coding scheme.

Our scheme consists of a classical source coder, two WZ coders, and a linear estimator. High-dimensional entropy-coded dithered quantization (ECDQ) is employed for source coding and high dimensional SW-coded dithered quantization is employed for Wyner-Ziv coding. In the following analysis, we assume that both of them are optimal in the sense of achieving the rate-distortion bound and the WZ bound.

First, *Classical Source Encoder* quantizes Y_2^n to $B_{21}^n = Q_{21}(Y_2^n)$ using *Dithered Quantizer II*, and compresses B_{21}^n using *Entropy Encoder*. The output message W_{21} is transmitted at rate $nR_{21} \geq H(B_{21}^n)$. At decoder side, W_{21} is losslessly decompressed to $\hat{B}_{21}^n = B_{21}^n$ and *Source Decoder II* uses $\hat{B}_{21}^n$ to reconstruct Y_2^n as $\tilde{Y}_{21}^n$. By exploring the remained correlation between $\tilde{Y}_{21}^n$ and Y_1^n, *Slepian-Wolf Encoder I* compresses $B_1^n = Q_1(Y_1^n)$, the quantization output of Y_1^n, from its entropy $H(B_1^n)$ down to the SW limit $nR_1 \geq H(B_1^n|\tilde{Y}_{21}^n)$. Using $\tilde{Y}_{21}^n$ as side information, *Wyner-Ziv Decoder I* generates $\hat{B}_1^n$, the reconstruction of B_1^n, and decodes it to $\tilde{Y}_1^n$. Then, $\tilde{Y}_{21}^n$ and $\tilde{Y}_1^n$ are

linearly combined to $\tilde{Y}_c^n$ (which will be used as side information for coding B_{22}^n), i.e.,

$$\tilde{Y}_c^n = \alpha_{12}\tilde{Y}_{21}^n + \beta_{12}\tilde{Y}_1^n, \tag{5.1}$$

where α_{12} and β_{12} are optimal estimation coefficients for Y_2^n. Finally, $B_{22}^n = Q_{22}(Y_2^n)$ is compressed to rate $nR_{22} \geq H(B_{22}^n|\tilde{Y}_c^n)$. *Wyner-Ziv Decoder II* then sequentially decodes $\hat{B}_{22}^n$ and $\tilde{Y}_{22}^n$. Given $\tilde{Y}_{21}^n$, $\tilde{Y}_1^n$, and $\tilde{Y}_{22}^n$, *Linear Estimator* reproduces Y_1^n and Y_2^n in the direct case, or X^n in the indirect case, using linear combination of the inputs:

$$\hat{Y}_1^n = \alpha_{y1}\tilde{Y}_1^n + \beta_{y1}\tilde{Y}_{21}^n + \gamma_{y1}\tilde{Y}_{22}^n, \tag{5.2}$$

$$\hat{Y}_2^n = \alpha_{y2}\tilde{Y}_1^n + \beta_{y2}\tilde{Y}_{21}^n + \gamma_{y2}\tilde{Y}_{22}^n, \tag{5.3}$$

$$\hat{X}^n = \alpha_x\tilde{Y}_1^n + \beta_x\tilde{Y}_{21}^n + \gamma_x\tilde{Y}_{22}^n. \tag{5.4}$$

Because optimal dithered quantization produces Gaussian quantization noise which is independent of the source, we may assume that $(X_i, Y_{1,i}, Y_{2,i}, \tilde{Y}_{1,i}, \tilde{Y}_{21,i}, \tilde{Y}_{22,i}, \tilde{Y}_{c,i})$ are jointly Gaussian. This leads to the equality $\frac{1}{n}H(B_{22}^n|\tilde{Y}_{21}^n, \tilde{Y}_1^n) = \frac{1}{n}H(B_{22}^n|\tilde{Y}_c^n)$, hence no rate loss is introduced by using $\tilde{Y}_c^n$ as side information for B_{22}^n. The linear estimators (5.2), (5.3), and (5.4) are also optimal in this jointly Gaussian case.

B. Theoretical Analysis

Define the quantization errors of the three quantizers as

$$E_1^n = \tilde{Y}_1^n - Y_1^n, \tag{5.5}$$

$$E_{21}^n = \tilde{Y}_{21}^n - Y_2^n \tag{5.6}$$

$$E_{22}^n = \tilde{Y}_{22}^n - Y_2^n. \tag{5.7}$$

Then we can write the relations between one sample block of random variables in the ideal jointly Gaussian case as:

$$
\begin{aligned}
Y_1^n &= X^n + N_1^n; && (5.8)\\
Y_2^n &= X^n + N_2^n; && (5.9)\\
\tilde{Y}_{21}^n &= Y_2^n + E_1^n = X^n + N_2^n + E_1^n; && (5.10)\\
\tilde{Y}_1^n &= Y_1^n + E_2^n = X^n + N_1^n + E_2^n; && (5.11)\\
\tilde{Y}_{22}^n &= Y_2^n + E_3^n = X^n + N_2^n + E_3^n; && (5.12)\\
\tilde{Y}_c^n &= \alpha_{12}\tilde{Y}_2^n + \beta_{12}\tilde{Y}_1^n; && (5.13)\\
\hat{Y}_1^n &= \alpha_{y1}\tilde{Y}_2^n + \beta_{y1}\tilde{Y}_1^n + \gamma_{y1}\tilde{Y}_{22}^n; && (5.14)\\
\hat{Y}_2^n &= \alpha_{y2}\tilde{Y}_2^n + \beta_{y2}\tilde{Y}_1^n + \gamma_{y2}\tilde{Y}_{22}^n; && (5.15)\\
\hat{X}^n &= \alpha_x\tilde{Y}_2^n + \beta_x\tilde{Y}_1^n + \gamma_x\tilde{Y}_{22}^n; && (5.16)
\end{aligned}
$$

where $\{X^n, N_1^n, N_2^n, E_1^n, E_2^n, E_3^n\}$ are mutually independent and a Markov chain $\tilde{Y}_1^n \rightarrow Y_1^n \rightarrow X^n \rightarrow Y_2^n \rightarrow (\tilde{Y}_{21}^n, \tilde{Y}_{22}^n)$ is satisfied. The covariance matrix of the vector of random variables $(X, Y_1, Y_2, \tilde{Y}_{21}, \tilde{Y}_1, \tilde{Y}_{22})^T$ can be written as (see Table II)

Table II. The covariance matrix

$E(\cdot,\cdot)$	X	Y_1	Y_2	$\tilde{Y}_{21}$	$\tilde{Y}_1$	$\tilde{Y}_{22}$
X	σ_x^2	σ_x^2	σ_x^2	σ_x^2	σ_x^2	σ_x^2
Y_1	σ_x^2	$\sigma_x^2+\sigma_n^2$	σ_x^2	σ_x^2	$\sigma_x^2+\sigma_n^2$	σ_x^2
Y_2	σ_x^2	σ_x^2	$\sigma_x^2+\sigma_n^2$	$\sigma_x^2+\sigma_n^2$	σ_x^2	$\sigma_x^2+\sigma_n^2$
$\tilde{Y}_{21}$	σ_x^2	σ_x^2	$\sigma_x^2+\sigma_n^2$	$\sigma_x^2+\sigma_n^2+d_{21}$	σ_x^2	$\sigma_x^2+\sigma_n^2$
$\tilde{Y}_1$	σ_x^2	$\sigma_x^2+\sigma_n^2$	σ_x^2	σ_x^2	$\sigma_x^2+\sigma_n^2+d_1$	σ_x^2
$\tilde{Y}_{22}$	σ_x^2	σ_x^2	$\sigma_x^2+\sigma_n^2$	$\sigma_x^2+\sigma_n^2$	σ_x^2	$\sigma_x^2+\sigma_n^2+d_{22}$

where d_1, d_{21}, d_{22} are the average quantization distortions defined by

$$d_1 = \frac{1}{n}\sum_{i=1}^{n}(Y_{1,i} - \tilde{Y}_{1,i})^2 = \frac{1}{n}\sum_{i=1}^{n} E_{1,i}^2, \tag{5.17}$$

$$d_{21} = \frac{1}{n}\sum_{i=1}^{n}(Y_{21,i} - \tilde{Y}_{21,i})^2 = \frac{1}{n}\sum_{i=1}^{n} E_{21,i}^2, \tag{5.18}$$

$$d_{22} = \frac{1}{n}\sum_{i=1}^{n}(Y_{22,i} - \tilde{Y}_{22,i})^2 = \frac{1}{n}\sum_{i=1}^{n} E_{22,i}^2. \tag{5.19}$$

Given the covariance matrix, the jointly Gaussian random variables are completely defined. Before we state the two theorems, we first derive the combination coefficients which are the key parameters in the joint decoder. This is done by applying projection theorem.

1. Compute α_{12} and β_{12} in $\tilde{Y}_c = \alpha_{12}\tilde{Y}_{21} + \beta_{12}\tilde{Y}_1$ to minimize $\mathrm{E}\{d(\tilde{Y}_c, Y_2)\}$.

   Solution: Due to orthogonal properties for optimal estimation, we have

$$\begin{cases} E\{(Y_2 - \tilde{Y}_c)\tilde{Y}_c\} &= 0 \\ E\{(Y_2 - \tilde{Y}_c)\tilde{Y}_1\} &= 0 \end{cases}$$

$$\Rightarrow \begin{cases} (\sigma_x^2 + \sigma_n^2 + d_{21}) & \alpha_{12} & + & \sigma_x^2 & \beta_{12} &= & \sigma_x^2 + \sigma_n^2 \\ \sigma_x^2 & \alpha_{12} & + & (\sigma_x^2 + \sigma_n^2 + d_1) & \beta_{12} &= & \sigma_x^2 \end{cases}$$

$$\Rightarrow \begin{cases} \alpha_{12} &= (\sigma_x^2 + \sigma_n^2)(\sigma_x^2 + \sigma_n^2 + d_1) - \sigma_x^4 \\ \beta_{12} &= \sigma_x^2 d_{21} \end{cases} \Big/ \Delta \tag{5.20}$$

   where $\Delta = (\sigma_x^2 + \sigma_n^2 + d_{21})(\sigma_x^2 + \sigma_n^2 + d_1) - \sigma_x^4$.

2. Compute α_{y1}, β_{y1}, and γ_{y1} in $\hat{Y}_1 = \alpha_{y1}\tilde{Y}_2 + \beta_{y1}\tilde{Y}_1^* + \gamma_{y1}\tilde{Y}_{22}^*$ to minimize $\mathrm{E}\{d(\hat{Y}_1, Y_1)\}$.

   Solution:

$$\begin{cases} E\{(Y_1 - \hat{Y}_1)\tilde{Y}_{21}\} &= 0 \\ E\{(Y_1 - \hat{Y}_1)\tilde{Y}_1\} &= 0 \\ E\{(Y_1 - \hat{Y}_1)\tilde{Y}_{22}\} &= 0 \end{cases}$$

$$\Rightarrow \begin{cases} (\sigma_x^2+\sigma_n^2+d_{21}) & \alpha_{y1} & + & \sigma_x^2 & \beta_{y1} & + & (\sigma_x^2+\sigma_n^2) & \gamma_{y1} & = & \sigma_x^2 \\ \sigma_x^2 & \alpha_{y1} & + & (\sigma_x^2+\sigma_n^2+d_1) & \beta_{y1} & + & \sigma_x^2 & \gamma_{y1} & = & \sigma_x^2+\sigma_n^2 \\ (\sigma_x^2+\sigma_n^2) & \alpha_{y1} & + & \sigma_x^2 & \beta_{y1} & + & (\sigma_x^2+\sigma_n^2+d_{22}) & \gamma_{y1} & = & \sigma_x^2 \end{cases}$$

$$\Rightarrow \begin{cases} \alpha_{y1} &=& \frac{\sigma_x^2 d_1}{\Delta^*} \cdot \frac{d_2^*}{d_{21}} \\ \beta_{y1} &=& \frac{(\sigma_x^2+\sigma_n^2)(\sigma_x^2+\sigma_n^2+d_2^*)-\sigma_x^4}{\Delta^*} \\ \gamma_{y1} &=& \frac{\sigma_x^2 d_1}{\Delta^*} \cdot \frac{d_2^*}{d_{22}} \end{cases} \tag{5.21}$$

where $d_2^* = \frac{d_{21}d_{22}}{d_{21}+d_{22}}$, $\Delta^* = (\sigma_x^2+\sigma_n^2+d_2^*)(\sigma_x^2+\sigma_n^2+d_1)-\sigma_x^4$.

3. Compute α_{y2}, β_{y2}, and γ_{y2} in $\hat{Y}_2 = \alpha_{y2}\tilde{Y}_{21} + \beta_{y2}\tilde{Y}_1^* + \gamma_{y2}\tilde{Y}_{22}^*$ to minimize $\mathrm{E}\{d(\hat{Y}_2, Y_2)\}$.

   Solution:

$$\begin{cases} E\{(Y_2-\hat{Y}_2)\tilde{Y}_{21}\} &=& 0 \\ E\{(Y_2-\hat{Y}_2)\tilde{Y}_1^*\} &=& 0 \\ E\{(Y_2-\hat{Y}_2)\tilde{Y}_{22}\} &=& 0 \end{cases}$$

$$\Rightarrow \begin{cases} (\sigma_x^2+\sigma_n^2+d_{21}) & \alpha_{y1} & + & \sigma_x^2 & \beta_{y1} & + & (\sigma_x^2+\sigma_n^2) & \gamma_{y1} & = & \sigma_x^2+\sigma_n^2 \\ \sigma_x^2 & \alpha_{y1} & + & (\sigma_x^2+\sigma_n^2+d_1) & \beta_{y1} & + & \sigma_x^2 & \gamma_{y1} & = & \sigma_x^2 \\ (\sigma_x^2+\sigma_n^2) & \alpha_{y1} & + & \sigma_x^2 & \beta_{y1} & + & (\sigma_x^2+\sigma_n^2+d_{22}) & \gamma_{y1} & = & \sigma_x^2+\sigma_n^2 \end{cases}$$

$$\Rightarrow \begin{cases} \alpha_{y2} &=& \frac{(\sigma_x^2+\sigma_n^2)(\sigma_x^2+\sigma_n^2+d_1)-\sigma_x^4}{\Delta^*} \cdot \frac{d_2^*}{d_{21}} \\ \beta_{y2} &=& \frac{\sigma_x^2 d_2^*}{\Delta^*} \\ \gamma_{y2} &=& \frac{(\sigma_x^2+\sigma_n^2)(\sigma_x^2+\sigma_n^2+d_1)-\sigma_x^4}{\Delta^*} \cdot \frac{d_2^*}{d_{22}} \end{cases} \tag{5.22}$$

4. Compute α_x, β_x, and β_x in $\hat{Y}_1 = \alpha_x\tilde{Y}_2 + \beta_x\tilde{Y}_1^* + \gamma_x\tilde{Y}_{22}^*$ to minimize $\mathrm{E}\{d(\hat{X}, X)\}$.

Solution:

$$\begin{cases} E\{(X-\hat{Y}_2)\tilde{Y}_{21}\} &= 0 \\ E\{(X-\hat{Y}_2)\tilde{Y}_1^*\} &= 0 \\ E\{(X-\hat{Y}_2)\tilde{Y}_{22}\} &= 0 \end{cases}$$

$$\Rightarrow \begin{cases} (\sigma_x^2+\sigma_n^2+d_{21}) & \alpha_{y1} & + & \sigma_x^2 & \beta_{y1} & + & (\sigma_x^2+\sigma_n^2) & \gamma_{y1} &= \sigma_x^2 \\ \sigma_x^2 & \alpha_{y1} & + & (\sigma_x^2+\sigma_n^2+d_1) & \beta_{y1} & + & \sigma_x^2 & \gamma_{y1} &= \sigma_x^2 \\ (\sigma_x^2+\sigma_n^2) & \alpha_{y1} & + & \sigma_x^2 & \beta_{y1} & + & (\sigma_x^2+\sigma_n^2+d_{22}) & \gamma_{y1} &= \sigma_x^2 \end{cases}$$

$$\Rightarrow \begin{cases} \alpha_x &= \frac{\sigma_x^2(\sigma_n^2+d_1)}{\Delta^*} \cdot \frac{d_2^*}{d_{21}} \\ \beta_x &= \frac{\sigma_x^2(\sigma_n^2+d_2^*)}{\Delta^*} \\ \gamma_x &= \frac{\sigma_x^2(\sigma_n^2+d_1)}{\Delta^*} \cdot \frac{d_2^*}{d_{22}} \end{cases} \tag{5.23}$$

Due to rate-distortion theory and the WZ theorem [2], the transmission rates (R_1, R_{21}, R_{22}) of our scheme satisfy

$$nR_1 \geq I(Y_1^n;\tilde{Y}_1^n) - I(\tilde{Y}_1^n;\tilde{Y}_{21}^n), \tag{5.24}$$

$$nR_{21} \geq I(Y_2^n;\tilde{Y}_{21}^n), \tag{5.25}$$

$$nR_{22} \geq I(Y_2^n;\tilde{Y}_{22}^n) - I(\tilde{Y}_{22}^n;\tilde{Y}_c^n). \tag{5.26}$$

Note that for jointly Gaussian random variables X and Y, $I(X;Y) = -\frac{1}{2}\log(1-\rho_{xy}^2)$, where $\rho_{xy}^2 = \frac{E^2(XY)}{E(X^2)E(Y^2)}$. Hence we get

$$\rho_{Y_2,\tilde{Y}_{21}}^2 = \frac{E^2(Y_2\tilde{Y}_{21})}{E(Y_2^2)E(\tilde{Y}_{21}^2)} = \frac{(\sigma_x^2+\sigma_n^2)^2}{(\sigma_x^2+\sigma_n^2)(\sigma_x^2+\sigma_n^2+d_{21})} = \frac{\sigma_x^2+\sigma_n^2}{\sigma_x^2+\sigma_n^2+d_{21}}; \tag{5.27}$$

$$\rho_{Y_1,\tilde{Y}_1}^2 = \frac{\sigma_x^2+\sigma_n^2}{\sigma_x^2+\sigma_n^2+d_1}; \tag{5.28}$$

$$\rho_{\tilde{Y}_{21},\tilde{Y}_1}^2 = \frac{\sigma_x^4}{(\sigma_x^2+\sigma_n^2+d_{21})(\sigma_x^2+\sigma_n^2+d_1)}; \tag{5.29}$$

$$\rho_{Y_2,\tilde{Y}_{22}}^2 = \frac{\sigma_x^2+\sigma_n^2}{\sigma_x^2+\sigma_n^2+d_{22}}; \tag{5.30}$$

$$\rho_{\tilde{Y}_c,\tilde{Y}_{22}}^2 = \frac{\left(\alpha_{12}(\sigma_x^2+\sigma_n^2)+\beta_{12}\sigma_x^2\right)^2}{(\alpha_{12}^2(\sigma_x^2+\sigma_n^2+d_{21})+\beta_{12}(\sigma_x^2+\sigma_n^2+d_1)+2\alpha_{12}\beta_{12}\sigma_x^2)\,(\sigma_x^2+\sigma_n^2+d_{22})}. \tag{5.31}$$

Using (5.27) – (5.31) in (5.24) – (5.26), we derive the rates R_1, R_{21}, R_{22} as

$$\begin{aligned} R_{21} &\geq I(Y_2;\tilde{Y}_{21}) \\ &= -\frac{1}{2}\log\left(1-\rho^2_{Y_2,\tilde{Y}_{21}}\right) = \frac{1}{2}\log\left(\frac{\sigma_x^2+\sigma_n^2+d_{21}}{d_{21}}\right); \qquad (5.32) \\ R_1 &\geq I(Y_1;\tilde{Y}_1) - I(\tilde{Y}_{21};\tilde{Y}_1) \\ &= \frac{1}{2}\log\left(\frac{1-\rho^2_{\tilde{Y}_{21},\tilde{Y}_1}}{1-\rho^2_{Y_1,\tilde{Y}_1}}\right) = \frac{1}{2}\log\left(\frac{\Delta}{d_1(\sigma_x^2+\sigma_n^2+d_{21})}\right); \qquad (5.33) \\ R_{22} &\geq I(Y_2;\tilde{Y}_{22}) - I(\tilde{Y}_c;\tilde{Y}_{22}) \\ &= \frac{1}{2}\log\left(\frac{1-\rho_{\tilde{Y}_c,\tilde{Y}_{22}^2}}{1-\rho^2_{Y_2,\tilde{Y}_{22}}}\right) = \frac{1}{2}\log\left(\frac{\Delta^*}{\Delta}\cdot\frac{d_{21}}{d_2^*}\right); \qquad (5.34) \end{aligned}$$

The overall average distortion can be expressed as

$$\begin{aligned} D &= E\left\{(X-\hat{X})^2\right\} = E\left\{(X-\alpha_x\tilde{Y}_2-\beta_x\tilde{Y}_1^*-\gamma_x\bar{Y}_2^*)^2\right\} \\ &= \frac{\sigma_x^2(\sigma_n^2+d_2^*)(\sigma_n^2+d_1)}{\Delta^*}; \qquad (5.35) \\ D_1 &= E\left\{d(Y_1-\hat{Y}_1)\right\} = E\left\{(Y_1-\alpha_{y1}\tilde{Y}_2-\beta_{y1}\tilde{Y}_1^*-\gamma_{y1}\bar{Y}_2^*)^2\right\} \\ &= \frac{d_1((2\sigma_x^2+\sigma_n^2)\sigma_n^2+d_2^*(\sigma_x^2+\sigma_n^2))}{\Delta^*}; \qquad (5.36) \\ D_2 &= E\left\{d(Y_2-\hat{Y}_2)\right\} = E\left\{(Y_2-\alpha_{y2}\tilde{Y}_2-\beta_{y2}\tilde{Y}_1^*-\gamma_{y2}\bar{Y}_2^*)^2\right\} \\ &= \frac{d_2^*((2\sigma_x^2+\sigma_n^2)\sigma_n^2+d_1(\sigma_x^2+\sigma_n^2))}{\Delta^*}; \qquad (5.37) \end{aligned}$$

The following two theorems show that the proposed scheme can approach any point on the inner sum rate bound in both direct and indirect multiterminal settings.

Theorem 1 (*indirect case*) Given the source variance σ_x^2, the noise power σ_n^2, and a distortion constraint $E[(X,\hat{X})^2] \leq D^*$, any rate pair (R_1^*, R_2^*) that satisfies

$$\begin{aligned} R_1^*, R_2^* &\geq r \quad = \frac{1}{2}\log^+[\frac{2\sigma_x^2}{\sigma_x^2+D^*}\cdot(1-\frac{\sigma_n^2(\sigma_x^2-D^*)}{2\sigma_x^2D^*})^{-1}], \qquad (5.38) \\ R_1^*+R_2^* &= r_{sum} = \frac{1}{2}\log^+[\frac{\sigma_x^2}{D^*}\cdot(1-\frac{\sigma_n^2(\sigma_x^2-D^*)}{2\sigma_x^2D^*})^{-2}], \qquad (5.39) \end{aligned}$$

is achievable with the proposed scheme.

Proof: We prove the theorem by construction. Let

$$d_1 = \frac{2\sigma_x^2 D^*}{\sigma_x^2 - D^*} - \sigma_n^2, \tag{5.40}$$

$$d_{21} = \frac{\sigma_x^4}{\sigma_x^2 + \sigma_n^2 + d_1(1 - 2^{2R_1^*})} - \sigma_x^2 - \sigma_n^2, \tag{5.41}$$

$$d_{22} = (\frac{1}{d_{21}} - \frac{1}{d_{21}})^{-1}. \tag{5.42}$$

Hence, $d_2^* = \frac{d_{21}d_{22}}{d_{21}+d_{22}} = d_1$. According to (5.32) – (5.35), we have

$$\begin{aligned} R_1 &\geq \frac{1}{2}\log\left(\frac{\Delta}{d_1(\sigma_x^2 + \sigma_n^2 + d_{21})}\right) \\ &= \frac{1}{2}\log\left(\frac{1}{d_1}(\sigma_x^2 + \sigma_n^2 + d_1 - \frac{\sigma_x^4}{\sigma_x^2 + \sigma_n^2 + d_{21}})\right) \\ &= \frac{1}{2}\log\left(\frac{1}{d_1}(\sigma_x^2 + \sigma_n^2 + d_1 - (\sigma_x^2 + \sigma_n^2 + d_1(1 - 2^{2R_1^*})))\right) \\ &= R_1^*; \end{aligned} \tag{5.43}$$

$$\begin{aligned} R_2 = R_{21} + R_{22} &\geq \frac{1}{2}\log\left(\frac{\sigma_x^2 + \sigma_n^2 + d_{21}}{d_{21}} \cdot (\frac{\Delta^*}{\Delta} \cdot \frac{d_{21}}{d_2^*})\right) \\ &= \frac{1}{2}\log\left(\frac{\Delta^*}{d_2^* d_1}\right) - \frac{1}{2}\log(\frac{\Delta}{d_1(\sigma_x^2 + \sigma_n^2 + d_{21})}) \\ &= \frac{1}{2}\log\left(\frac{(\sigma_x^2 + \sigma_n^2 + d_1)^2 - \sigma_x^4}{d_1^2}\right) - R_1^* \\ &= \frac{1}{2}\log\left(\frac{(\sigma_x^2(\sigma_x^2 + D^*)/(\sigma_x^2 - D^*))^2 - \sigma_x^4}{(2\sigma_x^2 D^*/(\sigma_x^2 - D^*) - \sigma_n^2)^2}\right) - R_1^* \\ &= \frac{1}{2}\log\left(\frac{4\sigma_x^6 D^*}{(2\sigma_x^2 D^* - \sigma_n^2(\sigma_x^2 - D^*))^2}\right) - R_1^* \\ &= \frac{1}{2}\log\frac{\sigma_x^2}{D^*} - \log\left(1 - \frac{\sigma_n^2(\sigma_x^2 - D^*)}{2\sigma_x^2 D^*}\right) - R_1^* \\ &= r_{sum} - R_1^* \\ &= R_2^*; \end{aligned} \tag{5.44}$$

$$\begin{aligned} D &= \frac{\sigma_x^2(\sigma_n^2 + d_2^*)(\sigma_n^2 + d_1)}{\Delta^*} \\ &= \frac{\sigma_x^2(\sigma_n^2 + d_1)^2}{(\sigma_x^2 + \sigma_n^2 + d_1)^2 - \sigma_x^4} \end{aligned}$$

$$
\begin{aligned}
&= \frac{\sigma_x^2(\sigma_n^2 + d_1)}{2\sigma_x^2 + \sigma_n^2 + d_1} \\
&= \frac{\sigma_x^2 \cdot 2\sigma_x^2 D^*}{2\sigma_x^2(\sigma_x^2 - D^*) + 2\sigma_x^2 D^*} \\
&= \frac{\sigma_x^2 D^*}{(\sigma_x^2 - D^*) + D^*} \\
&= D^*. \qquad (5.45)
\end{aligned}
$$

Finally, it is easy to show that for any achievable triple (R_1^*, R_2^*, D^*), there exist quantization step sizes such that quantization distortions d_1, d_{21}, d_{22} are positive. Thus, we can approach any point on the sum rate bound (4.24) – (4.25).

Theorem 2 (*direct case*) For jointly Gaussian sources (Y_1, Y_2) with variances $(\sigma_{y1}^2, \sigma_{y2}^2)$ and correlation coefficient ρ, given distortion constraints

$$E[(Y_1, \hat{Y}_1)^2] \le D_1^*, \quad E[(Y_2, \hat{Y}_2)^2] \le D_2^*. \qquad (5.46)$$

any rate pair (R_1^*, R_2^*) that satisfies

$$
\begin{aligned}
R_1^* &\ge \frac{1}{2}\log[\frac{\sigma_{y_1}^2}{D_1^*}(1 - \rho^2 + \rho^2 2^{-2R_2^*})], \qquad (5.47) \\
R_2^* &\ge \frac{1}{2}\log[\frac{\sigma_{y_2}^2}{D_2^*}(1 - \rho^2 + \rho^2 2^{-2R_1^*})], \qquad (5.48) \\
R_1 + R_2 &= r_{sum} = \frac{1}{2}\log[(1-\rho^2)\frac{\beta_{max}\sigma_{y_1}^2\sigma_{y_2}^2}{2D_1^* D_2^*}] \qquad (5.49)
\end{aligned}
$$

is achievable with the proposed scheme.

Proof: Define

$$
\begin{aligned}
\sigma_x^2 &= 1, \quad \sigma_n^2 = \sigma_x^2 \cdot \tfrac{1-\rho}{\rho}; \\
k_1 &= \tfrac{\sqrt{\sigma_x^2+\sigma_n^2}}{\sigma_{y1}}, \quad k_2 = \tfrac{\sqrt{\sigma_x^2+\sigma_n^2}}{\sigma_{y2}}; \qquad (5.50) \\
D_1' &= k_1^2 D_1^*, \quad D_2' = k_2^2 D_2^*;
\end{aligned}
$$

We first scale the sources (Y_1, Y_2) to $(Y_1' = k_1 Y_1, Y_2' = k_2 Y_2)$, which are of the same variance $\sigma_x^2 + \sigma_n^2$ and correlation coefficient ρ. Then we use the proposed scheme to

compress (Y_1', Y_2') according to target distortion pair (D_1', D_2'). Let

$$\begin{aligned} d_1 &= \frac{(\sigma_x^2+\sigma_n^2+d_2^{\Delta})(\sigma_x^2+\sigma_n^2)-\sigma_x^4}{(1-\rho^2)d_2^{\Delta}\beta_{max}(\sigma_x^2+\sigma_n^2)^2/(2D_1'D_2')-(\sigma_x^2+\sigma_n^2+d_2^{\Delta})}; \\ &= \frac{2D_1'((\sigma_x^2+\sigma_n^2)^2-\sigma_x^4)}{((\sigma_x^2+\sigma_n^2)^2-\sigma_x^4)\beta_{max}-2D_1'(\sigma_x^2+\sigma_n^2)} \qquad (5.51) \\ d_{21} &= \frac{\sigma_x^2}{\sigma_x^2+\sigma_n^2+d_1(1-2^{2R_1^*})}-\sigma_x^2-\sigma_n^2; \qquad (5.52) \\ d_{22} &= (\frac{1}{d_2^{\Delta}}-\frac{1}{d_1})^{-1}; \qquad (5.53) \end{aligned}$$

where

$$d_2^{\Delta} = \frac{2D_2'((\sigma_x^2+\sigma_n^2)^2-\sigma_x^4)}{((\sigma_x^2+\sigma_n^2)^2-\sigma_x^4)\beta_{max}-2D_2'(\sigma_x^2+\sigma_n^2)}$$

and β_{max} is defined by (4.32) with $\sigma_{y1}^2=\sigma_{y2}^2=\sigma_x^2+\sigma_n^2$, i.e.,

$$\beta_{max}=1+\sqrt{1+\frac{4\rho^2D_1'D_2'}{(1-\rho^2)^2\sigma_{y_1'}^2\sigma_{y_2'}^2}}=1+\sqrt{1+\frac{4\rho^2D_1'D_2'}{(1-\rho^2)^2(\sigma_x^2+\sigma_n^2)^2}} \qquad (5.54)$$

In (5.51), we use the fact

$$\beta_{max}^{-1}=(\beta_{max}-2)\cdot\frac{4\rho^2D_1'D_2'}{(1-\rho^2)^2(\sigma_x^2+\sigma_n^2)^2}. \qquad (5.55)$$

Using (5.32), (5.33), (5.34), (5.36), and (5.37), we have

$$\begin{aligned} R_1 &\geq \frac{1}{2}\log\left(\frac{\Delta}{d_1(\sigma_x^2+\sigma_n^2+d_{21})}\right) \\ &= \frac{1}{2}\log\left(\frac{1}{d_1}(\sigma_x^2+\sigma_n^2+d_1-\frac{\sigma_x^2}{\sigma_x^2+\sigma_n^2+d_{21}})\right) \\ &= R_1^*; \qquad (5.56) \\ R_2 &= R_{21}+R_{22} \geq \frac{1}{2}\log\left(\frac{\Delta^*}{d_1d_2^*}\right)-\frac{1}{2}\log\left(\frac{\Delta}{d_1(\sigma_x^2+\sigma_n^2+d_{21})}\right) \\ &= \frac{1}{2}\log\left(\frac{(\sigma_x^2+\sigma_n^2+d_2^*)(\sigma_x^2+\sigma_n^2+d_1)-\sigma_x^4}{d_1d_2^*}\right)-R_1^* \\ &= \frac{1}{2}\log\left(\frac{((\sigma_x^2+\sigma_n^2+d_2^*)(\sigma_x^2+\sigma_n^2)-\sigma_x^4)+d_1(\sigma_x^2+\sigma_n^2+d_2^*)}{d_1d_2^*}\right)-R_1^* \end{aligned}$$

$$
\begin{aligned}
&= \frac{1}{2}\log\left(\frac{\left((1-\rho^2)\beta_{max}(\sigma_x^2+\sigma_n^2)^2\frac{d_2^*}{2D_1'D_2'}-(\sigma_x^2+\sigma_n^2+d_2^*)+(\sigma_x^2+\sigma_n^2+d_2^*)\right)d_1}{d_1 d_2^*}\right)-R_1^* \\
&= \frac{1}{2}\log\left((1-\rho^2)\beta_{max}\frac{(\sigma_x^2+\sigma_n^2)^2}{2D_1'D_2'}\right)-R_1^* \\
&= \frac{1}{2}\log\left((1-\rho^2)\beta_{max}\frac{(\sigma_x^2+\sigma_n^2)^2}{2k_1^2D_1k_2^2D_2}\right)-R_1^* \\
&= r_{sum}-R_1^* \\
&= R_2^*; \qquad (5.57)
\end{aligned}
$$

$$
\begin{aligned}
D_1 &= \frac{d_1\left(((\sigma_x^2+\sigma_n^2)^2-\sigma_x^4)+d_2^*(\sigma_x^2+\sigma_n^2)\right)}{\Delta^*} \\
&= \frac{d_1 d_2^*}{\Delta^*}\cdot\left(\frac{((\sigma_x^2+\sigma_n^2)^2-\sigma_x^4)\beta_{max}-2D_2'(\sigma_x^2+\sigma_n^2)}{2D_2'}+(\sigma_x^2+\sigma_n^2)\right) \\
&= \frac{2D_1'D_2'}{(1-\rho^2)\beta_{max}(\sigma_x^2+\sigma_n^2)^2}\cdot\frac{((\sigma_x^2+\sigma_n^2)^2-\sigma_x^4)\beta_{max}}{2D_2'} \\
&= D_1' \qquad (5.58)
\end{aligned}
$$

$$
\begin{aligned}
D_2 &= \frac{d_2^*\left(((\sigma_x^2+\sigma_n^2)^2-\sigma_x^4)+d_1(\sigma_x^2+\sigma_n^2)\right)}{\Delta^*} \\
&= \frac{d_1 d_2^*}{\Delta^*}\cdot\left(\frac{((\sigma_x^2+\sigma_n^2)^2-\sigma_x^4)\beta_{max}-2D_1'(\sigma_x^2+\sigma_n^2)}{2D_1'}-(\sigma_x^2+\sigma_n^2)\right) \\
&= \frac{2D_1'D_2'}{(1-\rho^2)\beta_{max}(\sigma_x^2+\sigma_n^2)^2}\cdot\frac{((\sigma_x^2+\sigma_n^2)^2-\sigma_x^4)\beta_{max}}{2D_1'} \\
&= D_2'. \qquad (5.59)
\end{aligned}
$$

Hence (R_1^*, R_2^*) is achievable to compress (Y_1', Y_2') such that

$$E[(Y_1', \hat{Y}_1')^2] \le D_1', \qquad E[(Y_2', \hat{Y}_2')^2] \le D_2'. \qquad (5.60)$$

By scaling the reconstructed sources $(\hat{Y}_1', \hat{Y}_2')$ to $(\hat{Y}_1 = \hat{Y}_1'/k_1, \hat{Y}_2 = \hat{Y}_2'/k_2)$, the distortion constraints in (5.46) are satisfied. Thus, we can approach any point on the inner sum rate bound (5.47) – (5.49).

The two corner points on the achievable sum rate bounds of both direct and indirect multiterminal problems can be obtained when d_{21} or d_{22} is infinity. Indeed,

to achieve the corner point $(r_{sum}-r, r)$ in indirect case, we set R_1^* in (5.41) to $r_{sum}-r$; then d_{21} becomes infinity, and *Wyner-Ziv Encoder-Decoder I* degenerate to classical source encoder-decoder. To achieve $(r, r_{sum}-r)$, we set $R_1^* = r$; then $d_{22}=\infty$, and *Wyner-Ziv Encoder-Decoder II* disappear.In both cases, our scheme reduces to the asymmetric coding scheme of [37]. Similar conclusions can also be made for direct case.

C. Results

To implement high dimensional ECDQ, we resort to entropy-coded TCQ [31] scheme with dithered uniform codebook. Because the total rate is divided into three parts, we have to deal with low rate (e.g., less than one bit per sample) compression of quantization indices. Hence, to achieve fractional rates we employed the SWC-TCVQ scheme for Wyner-Ziv coding.

For the indirect multiterminal problem, source X and noises N_1 and N_2 are zero mean, jointly Gaussian, and mutually independent with variances $\sigma_x^2 = 1$, σ_n^2, and σ_n^2, respectively. Noisy observations are given by $Y_1 = X+N_1$ and $Y_2 = X+N_2$. We refer σ_x^2/σ_n^2 as the *correlation signal to noise ratio* (CSNR). We attempt to approach the middle point on the theoretical bound, that is $R_1 = R_2$, where R_1 and R_2 are rates used for compressing Y_1 and Y_2, respectively. For a given target distortion D and CSNR, by varying quantization step sizes of TCQ/TCVQ, we obtained quantization noises d_{21}, d_{21}, d_{22} given by (5.40), (5.41), and (5.42), respectively. The transmission rates with ideal Slepian-Wolf coding, i.e., $R_{21}=\frac{1}{n}H(B_{21}^n)$, $R_1=\frac{1}{n}H(B_1^n|\tilde{Y}_{21}^n)$, and $R_{22}=\frac{1}{n}H(B_{22}^n|\tilde{Y}_c^n)$ are computed using Monte Carlo simulations. Practical SW encoders are based on irregular LDPC codes of length 10^6. We assumed error-free transmission if probability of decoding error was less than 10^{-6}.

Simulation results for the average distortion $D^* = -21.83$ dB and CSNR=20dB together with the sum rate bound are showed in Figure 30. For the middle point, the loss in rate is about 0.29 bit per sample (b/s). Compared to results in [26] where the gap to the bound was roughly 2 dB in average distortion at 6 b/s, our results showed a much smaller gap of 0.22dB.

For the direct case, sources Y_1 and Y_2 are assumed to be jointly Gaussian with variances $\sigma_{y1}^2 = \sigma_{y2}^2 = \sigma_x^2 + \sigma_n^2$, and $\rho = \frac{\sigma_x^2}{\sigma_x^2+\sigma_n^2}$. For a given target distortion pair (D_{21}, D_1), we compute $\sigma_n^2 = \frac{1-\rho}{\rho}\sigma_x^2$, and the quantization distortions are set to the values given by (5.51)-(5.54) by varying the step sizes. Results and the theoretical bounds are shown in Figure 31. For the symmetric point, we lost 0.30 b/s in rate, or 0.91dB in distortion.

The loss of roughly 0.30 b/s for the middle point in both cases consists of a 0.03 b/s loss from classical source coding, two 0.13 b/s losses from Wyner-Ziv coding, and a very small loss from the jointly Gaussian assumption. This corresponds to the 0.15 b/s loss for the corner points where only one WZ coder is employed.

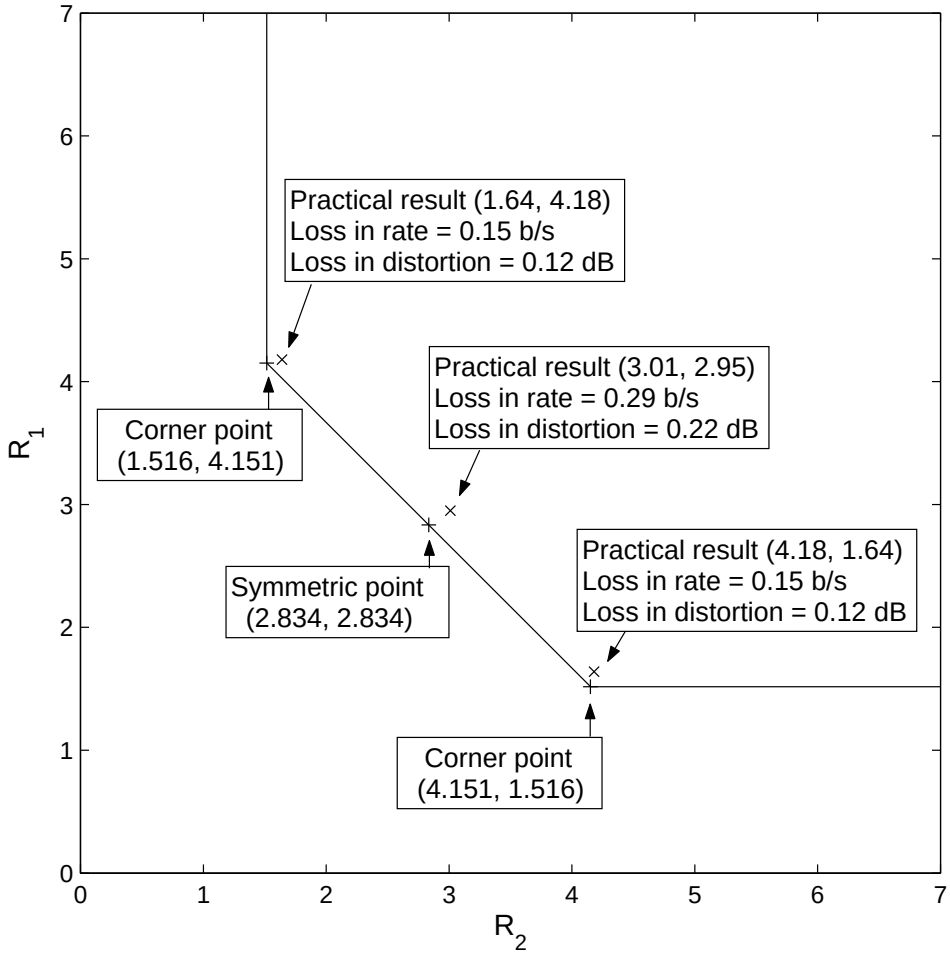

Fig. 30. Experimental results together with the sum rate bound for the indirect multiterminal problem. Target distortion is $D = -21.83$ dB and CSNR = 20 dB.

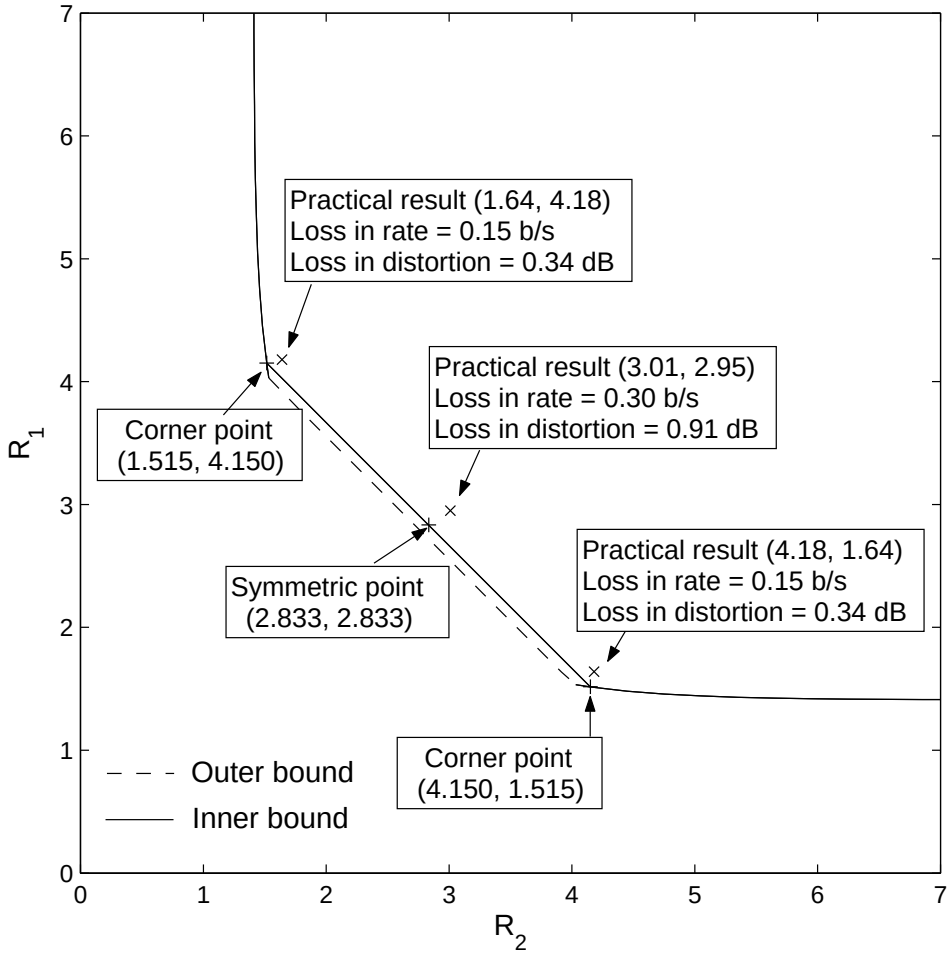

Fig. 31. Experimental results together with the inner and outer bounds for the direct multiterminal problem. Target distortions are $D_{21} = D_1 = -25.54$ dB and $\rho = 0.9901$.

CHAPTER VI

CONCLUSIONS

In this thesis, we first presented a SWC-TCQ scheme for quadratic Gaussian Wyner-Ziv coding, established its performance limit, made the connection of SWC-TCQ to ECTCQ, and performed practical code design. Practical designs perform 0.82 dB away from $D^*_{WZ}(R)$ at medium bit rates (e.g., ≥ 1.5 b/s). With 2-D tellis coded vector quantization, the performance gap to $D^*_{WZ}(R)$ is only 0.66 dB at 1.0 b/s and 0.47 dB at 3.3 b/s. Although SWC-TCQ is by far the best design, the small performance loss in SWC-TCQ comes from three aspects: suboptimality of TCQ over infinite-dimensional VQ, rate loss in practical LDPC code design, and inaccuracy of our discretization scheme.

We also presented a practical coding scheme for the quadratic Gaussian multiterminal problem that can approach the two corner points of the achievable rate region. It quantizes one observation and performs Wyner-Ziv coding on the second using the quantized version of the first as side information. Experimental results showed that performance of our scheme based on TCQ/TCVQ and irregular LDPC codes for Slepian-Wolf coding comes much closer to the theoretical limits than any other previous solution. Indeed, for CSNR in the range of 15 to 22 dB, and the sum-rate of 4 b/s, the obtained results are more than 2 dB better than previously reported and are within only 0.5 dB away from the theoretical limit. Such a competitive performance of our design comes from a successful restoration of the correlation among quantized observations, an efficient extraction of the key information from the encoding TCQ bitstreams and their effective combination with the available side information.

Following the idea of [29], we then proposed the *first* practical coding scheme based on source splitting, which can approach any point on the achievable bounds for

both the quadratic Gaussian direct and indirect multiterminal problems. We quantize the first source using entropy-coded TCQ, and then exploit Wyner-Ziv coding on the second source using the quantized version of the first as the side information at the decoder. The two quantized versions are linearly combined to form the side information for a second stage Wyner-Ziv coding of the first source. Finally, we reconstruct the source(s) using a linear estimator. We proved that in the ideal case when all random variables are jointly Gaussian, in both direct and indirect multiterminal settings, the proposed scheme is capable of trading off transmission rates among the two encoders and achieving any point on the inner sum rate bound. Simulation results showed that in the indirect case, our scheme based on TCQ/TCVQ and irregular LDPC codes for Slepian-Wolf coding performs significantly better than the scheme of [26]. However, to approach any non-corner point, we need two Wyner-Ziv coding components. This causes a small performance loss compared to asymmetric coding (corner points) where only one Wyner-Ziv coding is needed. Hence, we gained in flexibilities of rate allocation at the cost of higher complexity and performance loss. Although the direct and indirect multiterminal problems essentially differ, our scheme performs equally well in both settings with only small adjustments. At sum rate of 5.96 b/s, we lost roughly 0.30 b/s in both direct and indirect settings. This small performance loss, due to suboptimality of TCQ, rate loss in practical LDPC coding, and limitations of linear estimators can probably be further reduced by exploiting higher dimensional TCVQ, using density evolution in LDPC code design, and constructing non-linear estimators. Another possibility of improving the results is to employ channel code partitioning method introduced for Slepian-Wolf coding in [38]. This is a part of our ongoing research.

REFERENCES

[1] D. Slepian and J. Wolf, "Noiseless coding of correlated information sources," *IEEE Trans. Inform. Theory*, vol. 19, pp. 471-480, July 1973.

[2] A. Wyner and J. Ziv, "The rate-distortion function for source coding with side information at the decoder," *IEEE Trans. Inform. Theory*, vol. 22, pp. 1-10, Jan. 1976.

[3] S. S. Pradhan, J. Chou, and K. Ramchandran, "Duality between source coding and channel coding and its extension to the side information case," *IEEE Trans. Inform. Theory*, vol. 49, pp. 1181-1203, May 2003.

[4] M. Marcellin and T. Fischer, "Trellis coded quantization of memoryless and Gaussian-Markov sources", *IEEE Trans. Communications*, vol. 38, pp. 82-93, Jan. 1990.

[5] C. Berrou and A. Glavieux, "Near optimum error correcting coding and decoding: turbo-codes," *IEEE Trans. Communications*, vol. 44, pp. 1261-1271, Oct. 1996.

[6] D. MacKay, "Good error-correcting codes based on very sparse matrices," *IEEE Trans. Inform. Theory*, vol. 45, pp. 399-431, March 1999.

[7] R. Zamir and S. Shamai, "Nested linear/lattice codes for Wyner-Ziv encoding," in *Proc. IEEE Information Theory Workshop*, Killarney, Ireland, June 1998, pp. 92-93.

[8] S. Servetto, "Lattice quantization with side information," in *Proc. DCC'00*, Snowbird, UT, March 2000, pp. 510-519.

[9] A. Liveris, Z. Xiong, and C. Georghiades, "Nested turbo codes for the binary Wyner-Ziv problem," in *Proc. ICIP'03*, Barcelona, Spain, Sept. 2003, vol. 1, pp. 601-604.

[10] X. Wang, and M. T. Orchard, "Design of trellis codes for source coding with side information at the decoder," in *Proc. DCC'01*, Snowbird, UT, March 2001, pp. 361-370.

[11] S. S. Pradhan and K. Ramchandran, "Distributed source coding using syndromes (DISCUS): Design and construction," *IEEE Trans. Inform. Theory*, vol. 49, pp. 626-643, March 2003.

[12] J. Chou, S. S. Pradhan and K. Ramchandran, "Turbo and trellis-based constructions for source coding with side information," in *Proc. DCC'03*, Snowbird, UT, March 2003, pp. 33-42.

[13] Z. Xiong, A. Liveris, S. Cheng, and Z. Liu, "Nested quantization and Slepian-Wolf coding: A Wyner-Ziv coding paradigm for i.i.d. sources," in *Proc. IEEE Workshop on Statistical Signal Processing*, St. Louis, MO, Sept. 2003, pp. 399-402.

[14] A. Liveris, Z. Xiong and C. Georghiades, "Compression of binary sources with side information at the decoder using LDPC codes," *IEEE Communications Letters*, vol. 6, pp. 440-442, Oct. 2002.

[15] P. Mitran and J. Bajcsy, "Coding for the Wyner-Ziv problem with turbo-like codes," in *Proc. ISIT'02*, Lausanne, Switzerland, July 2002, p. 91.

[16] D. Rebollo-Monedero, R. Zhang, and B. Girod, "Design of optimal quantizers for distributed source coding," in *Proc. DCC'03*, Snowbird, UT, March 2003, pp.

13-22.

[17] T. Berger, "Multiterminal source coding," in *The Information Theory Approach to Communications*, G. Longo, Ed., New York: Springer-Verlag, 1977, pp. 171-231.

[18] Y. Oohama, "Gaussian multiterminal source coding," *IEEE Trans. Inform. Theory*, vol. 43, pp. 1912-1923, Nov. 1997.

[19] H. Viswanathan and T. Berger, "The quadratic Gaussian CEO problem," *IEEE Trans. Inform. Theory,* vol. 43, pp. 1549–1559, Sept. 1997.

[20] Y. Oohama, "The rate-distortion function for the quadratic Gaussian CEO problem," *IEEE Trans. Inform. Theory*, vol. 44, pp. 1057–1070, May 1998.

[21] S. Y. Tung, "Multiterminal rate-distortion theory," Ph.D. dissertation, School of Electrical Engineering, Cornell University, Ithaca, NY, 1977.

[22] H. Yamamoto and K. Itoh, "Source coding theory for multiterminal communication systems with a remote source," *Trans. IECE of Japan*, vol. E63, pp. 700-706, Oct. 1980.

[23] T.J. Flynn and R.M. Gray, "Encoding of correlated observations," *IEEE Trans. Inform. Theory,* vol. IT-33, pp. 773–787, Nov. 1987.

[24] J. Chen, X. Zhang, T. Berger, and S. B. Wicker, "The sum-rate distortion function and optimal rate allocation for the quadratic Gaussian CEO problem," *IEEE JSAC: Special Issue on Sensor Networks*, to appear.

[25] V. Prabhakaran, D. Tse, and K. Ramchandran, "Rate region of the quadratic Gaussian CEO problem," in *Proc. ISIT'04*, Chicago, IL, June 2004, p. 119.

[26] S. S. Pradhan and K. Ramchandran, "Generalized coset codes for symmetric distributed source coding," *submitted to IEEE Trans. Inform. Theory*, Feb. 2003.

[27] B. Rimoldi and R. Urbanke, "Asynchronous Slepian-Wolf coding via source-splitting," in *Proc. ISIT'97*, Ulm, Germany, June 1997, p. 271.

[28] T. P. Coleman, A. H. Lee, M. Médard, and M. Effros, "On some new approaches to practical Slepian-Wolf compression inspired by channel coding," in *Proc. DCC'04*, Snowbird, UT, March 2004, pp. 282-291.

[29] R. Zamir, S. Shamai, and U. Erez, "Nested linear/lattice codes for structured multiterminal binning," *IEEE Trans. Inform. Theory,* vol. 48, pp. 1250-1276, June 2002.

[30] G. Ungerboeck, "Channel coding with multilevel/phase signals," *IEEE Trans. Inform. Theory,* vol. IT-28, pp. 55-67, Jan. 1982.

[31] D. Taubman and M. Marcellin, *JPEG2000: Image Compression Fundamentals, Standards, and Practice*, Kluwer Academic Publishers, Norwell, MA, 2001.

[32] Y. Yang, S.Chen, Z. Xiong, and W. Zhao, "Wyner-Ziv coding based on TCQ and LDPC codes," in *Proc. of 37th Asilomar Conference on Signals, Systems, and Computers*, Pacific Grove, CA, Nov. 2003, vol. 1, pp. 825-829.

[33] M. Marcellin, "On entropy-constrained trellis coded quantization," *IEEE Trans. on Communications*, vol. 42, pp. 14-16, Jan. 1994.

[34] T. J. Richardson and R. L. Urbanke, "The capacity of low-density parity-check codes," *IEEE Trans. Inform. Theory,* vol. IT-47, pp. 599-618, Feb. 2001.

[35] T. J. Richardson, M. A. Shokrollahi, and R. L. Urbanke, "Design of capacity-approaching irregular low-density parity-check codes", *IEEE Trans. Inform. Theory,* vol. IT-47, pp. 619-637, Feb. 2001.

[36] S. S. Pradhan and K. Ramchandran, "Distributed source coding: symmetric rates and applications to sensor networks," in *Proc. DCC'00*, Snowbird, UT, March 2000, pp. 363-372.

[37] Y. Yang, V. Stanković, Z. Xiong, and W. Zhao, "Asymmetric code design for remote multiterminal source coding," in *Proc. DCC'04*, Snowbird, UT, March 2004, p. 572.

[38] V. Stanković, A. Liveris, Z. Xiong, and C. Georghiades, "Design of Slepian-Wolf codes by channel code partitioning," in *Proc. DCC'04*, Snowbird, UT, March 2004, pp. 302-311.

VITA

Name	Yang Yang
Education	Master of Science (August 2002 – August 2004)
	Major: Electrical Engineering
	Texas A&M University, College Station, TX 77840
	Bachelor of Science (September 1998 – July 2002)
	Major: Electrical Engineering
	Tsinghua University, Beijing, P. R. China
Permanent address	Department of Electrical Engineering,
	Texas A&M University, College Station, TX 77843

The typist for this thesis was Yang Yang.